UNIVERSITY OF SOUTHAMPTON

FACULTY OF PHYSICAL AND APPLIED SCIENCES

School of Physics and Astronomy

Exciton Condensates and Free Carriers in Microcavities and Coupled Quantum Well Structures

by

THOMAS TAYLOR

A thesis submitted for the degree of
Doctor of Philosophy

June 2012

UNIVERSITY OF SOUTHAMPTON

ABSTRACT

FACULTY OF PHYSICAL AND APPLIED SCIENCES
SCHOOL OF PHYSICS AND ASTRONOMY

Doctor of Philosophy

Exciton Condensates and Free Carriers in Microcavities and Coupled Quantum Well Structures

by Thomas Taylor

This thesis examines a series of effects associated with condensation in excitonic systems, and in particular in systems of microcavity exciton-polaritons and indirect excitons. A proposal is presented for a terahertz laser based on a microcavity system, in which a polariton condensate is formed, stimulating the terahertz transition from the $2p$ exciton state. An associated fundamental effect is predicted, in which the threshold to lasing is dependent on the statistics of the pump photons. The potential of hybrid Bose-Fermi systems for the study of coherent many-body phenomena is demonstrated, by modelling the effects of interaction between an excitonic condensate and a two-dimensional electron gas. The fermionic subsystem of electrons is first considered, and it is shown that a phase transition to superconductivity may exist due to pairing mediated by virtual excitations of the condensate, analogous to the phonon mechanism in conventional superconductors. The system is modelled within BCS theory, and the gap equation is solved numerically to yield the critical temperature. The complementary effects of the electron gas on the bosonic condensate are also studied; the effective interaction between the constituents of the condensate may be strongly modified, affecting the superfluid properties of the condensate, and leading to the appearance of a roton minimum in the dispersion of elementary excitations. In fact, the dispersion may be modified to the extent that the roton gap closes, creating an instability in the system - it is shown that this instability may be manifested as a transition to a supersolid phase.

Contents

List of Figures

Declaration of Authorship

I, Thomas Taylor, declare that the thesis entitled *Exciton Condensates and Free Carriers in Microcavities and Coupled Quantum Well Structures* and the work presented in the thesis are both my own, and have been generated by me as the result of my original research. I can confirm that:

- this work was done wholly or mainly while in candidature for a research degree at this University;
- where any part of this thesis has previously been submitted for a degree or any other qualification at this University or any other institution, this has been clearly stated;
- where I have consulted the published work of others, this is always clearly attributed;
- where I have quoted from the work of others, the source is always given. With the exception of such quotations, this thesis is entirely my own work;
- I have acknowledged all main sources of help;
- where the thesis is based on work done by myself jointly with others, I have made clear exactly what was done by others and what I have contributed myself;
- parts of this work have been published as:
  - I. A. Shelykh, T. Taylor and A. V. Kavokin. Rotons in a Hybrid Bose-Fermi System. *Physical Review Letters*, **105**(14):140402, 2010.
  - M. Matuszewski, T. Taylor and A. V. Kavokin. Exciton Supersolidity in Hybrid Bose-Fermi Systems. *Physical Review Letters*, **108**(6):060401, 2012.
  - F. P. Laussy, T. Taylor, I. A. Shelykh and A. V. Kavokin. Superconductivity with Excitons and Polaritons: Review and Extension. *Journal of Nanophotonics*, **6**:064502, 2012.
  - A. V. Kavokin, I. A. Shelykh, T. Taylor and M. M. Glazov. Vertical Cavity Surface Emitting Terahertz Laser. *Physical Review Letters*, **108**(19):197401, 2012.

Signed: ..... **Date:**.....

Acknowledgements

I would first and foremost like to thank Alexey Kavokin for his patient supervision during my PhD, and for introducing me to and enabling me to work on some extremely interesting physics.

Many thanks also to Fabrice Laussy, whom I worked with extensively during his time at Southampton, especially on the work that is presented in chapter three. I learnt a great deal from Fabrice and very much enjoyed working with him. I am grateful to Ivan Shelykh for his help and hospitality during visits to Reykjavik, to collaborate on the work presented in chapters three and four. Finally, thanks to Michał Matuszewski, who carried out the numerical work presented in chapter five.

Chapter 1

Introduction

The first experimental observation of a pure Bose-Einstein condensate (BEC) occurred over fifteen years ago, yet this beautiful demonstration of quantum coherence on macroscopic scales continues to generate intense interest. The subtleties of this phase and its links to other spontaneously coherent effects in many real systems are still not fully understood, especially when considering the generalisation of BEC to fermionic, strongly interacting, nonequilibrium or low-dimensional systems. The richness of the phenomena associated with condensation ensures that research will continue to be stimulated by the study of this effect.

While the observation of BEC in cold-atom systems is now routine, it is only relatively recently that condensation has been demonstrated in solid state systems. These systems present new opportunities and challenges; significantly higher critical temperatures and interesting new effects have been demonstrated, encouraging the development of applications of this quantum effect, however the specifics of these systems complicate the interpretation of experiments in terms of BEC.

In particular, exciton and exciton-polariton condensates are extremely interesting from both the fundamental and practical points of view, and work in these fields

has now moved beyond the simple demonstration of condensation, to considering the properties of condensates in these systems and the implications of complexities not considered in the textbook description of BEC. This has already led to a rapid advance in understanding and many novel observations and proposals, however the relative immaturity of this area promises much more, as the theory of these systems in particular is further developed.

One example of this advance is in the physics of hybrid Bose-Fermi systems, in which a mixture of particles with bosonic and fermionic statistics are present. In cold-atom systems, Bose-Fermi mixtures have been studied in order to simulate other condensed matter systems, or to examine completely new regimes. Excitonic systems[1] demonstrate many advantages over atomic systems, and have enormous potential both as highly controllable laboratories for understanding of fundamental questions, and as systems which have widespread potential application. Combined with the associated ability to tailor interactions, these systems are ideal for the study of exotic effects due to mixed Bose-Fermi statistics.

1.1 Thesis outline

The work in this thesis considers both fundamental and application-motivated topics: an exciting application of condensation in microcavity systems is proposed, and the potential of excitonic Bose-Fermi systems to exhibit sought after low temperature quantum effects in the solid state is also demonstrated.

In the remainder of this introductory chapter, the general physics of excitons and

[1] *Excitonic* is used in this thesis to encompass both systems of excitons and exciton-polaritons.

exciton-polaritons will be discussed, and the systems in which they are studied will be examined in more detail, in order to prepare for the particular effects studied later. Condensation will then be considered in general terms, leading on to the observation of condensation and associated effects in excitonic systems.

The second chapter demonstrates a new and important application of microcavity systems: the possibility of terahertz lasing from a compact device, which would be a major advance when compared to bulky far infrared lasers or quantum cascade lasers. The quantum theory developed also implies an interesting associated fundamental effect: that the laser threshold is dependent on the statistics of the pump.

The remainder of the thesis considers a particular class of excitonic system, in which a bosonic condensate interacts with free carriers, i.e. a Bose-Fermi mixture. The interactions between the different components lead to complex and interesting effects in both the bosonic and fermionic subsystems. In chapter three the fermionic subsystem of free carriers is considered - electrons in a two-dimensional electron gas (2DEG). It is shown that interaction with a condensate of excitons or exciton-polaritons may, remarkably, lead to superconductivity, and furthermore superconductivity in which the critical temperature scales with the condensate density. This implies the possibility of observing high temperature superconductivity in a suitably designed system, which would be a significant breakthrough in the understanding of non-conventional superconductivity.

Chapters four and five then examine the complementary aspect of these systems: the effect of the interaction with free carriers on the excitonic condensate and on its superfluid properties. Firstly, it is shown in chapter four that for relatively

strong Bose-Fermi coupling, the dispersion of excitations of the condensate may be qualitatively altered, developing a roton minimum due to the change in the effective excitonic interaction. This is interesting from a fundamental point of view, however it is more interesting when considering that the roton minimum may become lower in energy than the ground state, leading to an instability in the system. Hence in chapter five this possibility is examined and shown to herald a phase transition to a supersolid phase, an exotic quantum phase which has been widely studied only relatively recently.

Finally, the thesis is concluded by summarising and discussing the implications of this work, and how it could be extended.

1.2 Excitons and exciton-polaritons

An exciton is a Coulomb bound electron-hole pair, and the elementary excitation of a semiconductor. The idea of an exciton as a neutral quasiparticle was first introduced by Frenkel [1], in the context of low dielectric constant organic materials. In these sorts of materials, excitons have a relatively small size and large binding energy, and are called Frenkel excitons. Excitons in semiconductors have a larger size, extending over many lattice spacings, and a smaller binding energy, and are also eponymously named Wannier-Mott excitons, after the two scientists who first discussed excitons in semiconductors [2, 3].

In semiconductors, Wannier-Mott excitons[2] may be created optically, due to the absorption of an optical photon by a valence band electron, which is excited to

[2]Henceforth just referred to as excitons.

the conduction band, leaving behind a *hole* - a region of excess positive charge compared to the normal state of the valence band. Coulomb attraction may lead to binding of the electron and hole, and an exciton state which is therefore lowered in energy compared to the unbound state. The background potential of the crystal lattice can be neglected when considering these excitons, employing the usual effective mass approximation to describe excitons as free particles with parabolic dispersion, but with finite lifetime, due to the possibility of recombination of the electron and hole [4].

In the systems studied in this thesis, excitons are confined in one direction, and hence behave as quasiparticles free in two dimensions, with quantised energies and associated quantum numbers in the third dimension. This is achieved by confining excitons in quantum wells (QWs), which are quasi-2D potential wells, created by layering a semiconductor, such as GaAs, between a different semiconductor with a wider bandgap, such as AlGaAs. As a consequence of this confinement, momentum conservation in an optical transition needs to be satisfied only in the QW plane direction, and not along the direction of confinement. Hence QW excitons couple to photons with the same in-plane wavevector $\mathbf{k}_{\parallel}$ and arbitrary transverse wavenumber k_z, making the QW exciton more optically accessible than in bulk materials.

As mentioned already, excitons are usually created optically; this coupling to the light field is normally weak, and its influence on the exciton can therefore be neglected or treated as a perturbation. However, increasing the coupling between the exciton state and a resonant light field, at some point the normal modes of the system cease to be given by the exciton and photon modes. Instead, strong

coupling leads to anticrossing of the two dispersion relations and new mixed light-matter modes: exciton-polaritons[3] [5].

1.3 Microcavity exciton-polaritons

In order to achieve strong coupling between QW excitons and a light field, the light field must normally be confined in the direction of exciton confinement. This is realised using a microcavity, an optical Fabry-Pérot resonator with a scale in the confinement direction on the order of the wavelength of light. The light field is confined using distributed Bragg reflectors (DBRs), which create a stop band for transmission by alternating layers of high and low refractive indices, each with an optical thickness of $\lambda/4$. The DBRs act as high reflectance mirrors for wavelengths within the stop band, the centre of which is at the wavelength λ. Hence when two DBRs sandwich a region with an optical thickness a multiple of $\lambda/2$, a cavity resonance is formed at λ. There is a one-to-one correspondence between the incidence angle of light on the microcavity, and each resonant mode with in-plane wavenumber $k_{\|}$, allowing straightforward measurement of the cavity mode or polariton in-plane wavenumber. Fig. 1.1 shows a schematic of the microcavity system - note that the QW is placed at a maximum of the cavity mode, in order to maximise the exciton-photon coupling strength.

By tuning the cavity mode to be in resonance with the exciton transition, the strong coupling regime can be reached, where the polariton is formed as a new eigenmode of the system. In order to achieve strong coupling, the exciton-photon

[3]The exciton-polariton is henceforth simply referred to as the polariton.

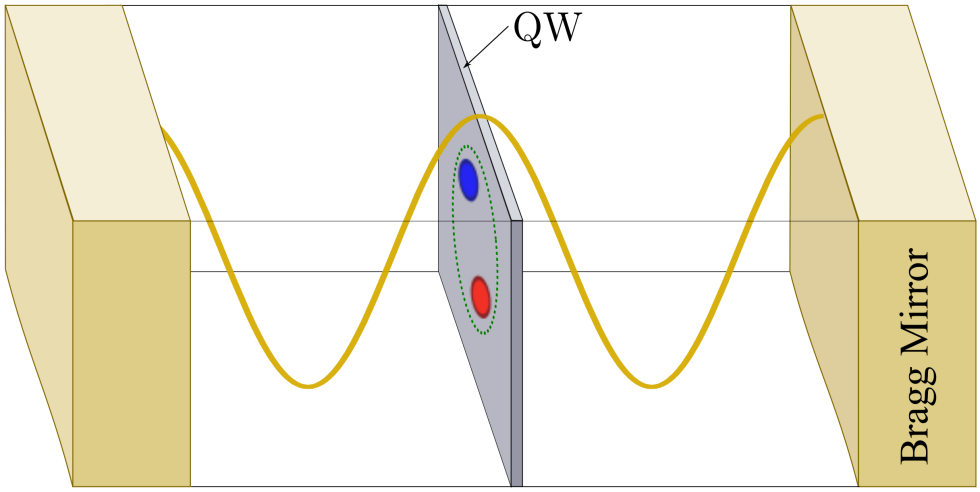

Figure 1.1: Schematic of a semiconductor microcavity.

coupling must dominate over the exciton and photon decay rates. If the coupling strength

$$g > \left| \frac{\gamma_{\mathrm{e}} - \gamma_{\mathrm{c}}}{2} \right| , \tag{1.1}$$

where γ_{e}^{-1}, γ_{c}^{-1} are the exciton, photon lifetimes, then anticrossing occurs between the exciton and photon modes, which is the signature of strong coupling [6].

The energy dispersion relation is given by

$$E_{\mathrm{U,L}}(k) = \frac{1}{2}(E_{\mathrm{X}}(k) + E_{\mathrm{C}}(k)) \pm \sqrt{\Delta(k)^2 + 4g^2} , \tag{1.2}$$

and is plotted in Fig. 1.2, for three values of the detuning, $\Delta(0)$, the difference in energy between the bare photon and exciton modes, with parabolic dispersion relations E_{C}, E_{X}, respectively. The two branches of the dispersion relation may be observed as two resonances in the reflection or transmission spectra, and the splitting between these resonances is called the vacuum-field Rabi splitting, $2g$.

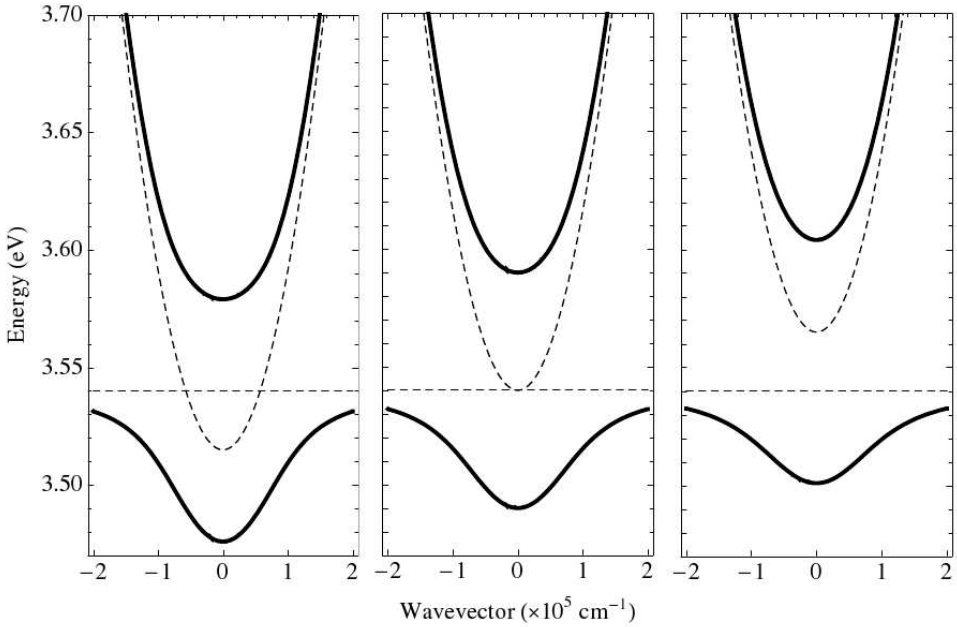

Figure 1.2: Dispersion of polaritons for (a) negative, (b) zero and (c) positive detuning between the bare photon and exciton modes, showing the upper and lower polariton branches. Dashed lines indicate the bare exciton and photon dispersions. Plotted for a GaN microcavity with typical parameters from [6, 8].

The lower polariton branch has an unusual shape, far from parabolic, which acts as a trap in reciprocal space, and results in the interesting and unique nonlinear dynamics of polaritons [7].

At low densities excitons, and therefore polaritons, have been shown to be good bosons, i.e. they obey Bose-Einstein statistics, and satisfy bosonic commutation relations:

$$\begin{aligned} \left[a_{\mathbf{k}}, a_{\mathbf{k}'}\right] &= \left[a^{\dagger}_{\mathbf{k}}, a^{\dagger}_{\mathbf{k}'}\right] = 0 \ , \\ \left[a_{\mathbf{k}}, a^{\dagger}_{\mathbf{k}'}\right] &= \delta_{\mathbf{k}\mathbf{k}'} - \mathrm{O}\left(n a_{\mathrm{B}}^{d}\right) \ , \end{aligned} \tag{1.3}$$

where d is the dimensionality of the system, a_{B} is the Bohr radius, and n is the concentration. Hence excitons can be considered good bosons when the exciton interparticle spacing is much larger than its Bohr radius: $n \ll a_{\mathrm{B}}^{-d}$. When this relation is no longer satisfied, the fermionic nature of the constituents making up the exciton becomes important. At a certain density, a system of electrons and holes undergoes a transition from bound excitons, to an electron-hole plasma [9]. This insulator-metal transition is called the Mott transition [10], and can be understood as occurring due to an increase of screening in the system, which prevents Coulomb binding of pairs, or due to filling of the phase space.

The bosonic nature of polaritons can be demonstrated by observing final state stimulation, where the presence of N particles in a final state enhances the scattering rate into that state by a factor of $N + 1$. This effect is important for formation of a condensate of polaritons, in assisting relaxation of polaritons to the ground state of the system, with zero in-plane wavevector. The effect was first observed in 1998 [11], in a CdTe-based experiment where polariton populations were generated by pumping the microcavity non-resonantly. This non-resonant pumping generates hot carriers which may then relax in energy to the lower polariton branch by emission of acoustic phonons. This process is an incoherent excitation of polaritons, and therefore may be used to examine *spontaneous* development of coherence in polariton systems, in contrast to resonant pumping, where coherence of polaritons is inherited from the pumping laser.

Stimulated scattering of polaritons has also been observed in parametric amplification experiments [12], where the lower polariton branch is pumped resonantly at the so-called 'magic angle', leading to coherent parametric scattering to signal

and idler states, where the signal state is the lowest energy region of the dispersion relation. Large amplification of a probe pulse which creates a seed population in the ground state is then observed, due to bosonic stimulation of the pump to signal transition. Stimulated scattering may also be observed without a seed pulse: by continuously pumping the pump state, a threshold power can be reached at which the transition to the signal state is itself enough to provide the seed population [13]. The ability to efficiently generate coherent populations of ground state polaritons was a crucial advance in the physics of microcavity polaritons, and will be examined in more detail below.

Microcavity polariton systems are very accessible experimentally, when compared to other solid state systems used to study quantum phases [14]. The distributions in time for both real and reciprocal space, as well as other properties of the polariton gas, can be measured directly due to the one-to-one correspondence between cavity polaritons and emitted photons. The light effective mass of the exciton-polariton results in high critical temperatures for quantum degeneracy, and structural disorder is also a less significant problem when compared to other systems, due to the extended coherence inherited from the photon.

The field of microcavity polaritons is growing quickly, due to the potential of polaritons for use in both fundamental and applied research, and has generated intense interest as an interdisciplinary field with aspects of quantum optics, photonics and condensed matter physics [15]. Quantum phases and macroscopic quantum coherence may be investigated in a variety of different ways, due to the control possible over all aspects of the system. Potential applications range from ultralow threshold lasers operating at room temperature [16] and terahertz lasers, as discussed later,

to even the development of a whole new class of optoelectronic devices utilising the polariton spin for information transfer [17, 18] - *spinoptronic* devices [19].

1.4 Cold exciton gases

While polaritons may exhibit quantum effects up to high temperatures, the comparatively high mass of the exciton means low temperatures are required to reach the regime of quantum degeneracy in systems of excitons. However, the exciton mass in typical semiconductors is still only of the order of the free electron mass, hence these low temperatures, in the few Kelvin range, are readily reached using standard helium refrigeration techniques.

In order to reach these temperatures within a gas of weakly interacting excitons, the exciton lifetime must be long enough to allow photoexcited excitons to cool towards the lattice temperature. By confining electrons and holes in separate QWs (in coupled QW structures, using an applied electric field perpendicular to the QW plane), the exciton lifetime can indeed be extended to the point where excitons can efficiently thermalise and cool within their lifetime, allowing formation of cold exciton gases, which do not rely on the light field for coherence properties. The lifetime is extended due to the spatial separation of electrons and holes, which reduces the overlap of their wavefunctions and therefore the likelyhood of recombination. Like polaritons, indirect excitons have been studied as an example of spontaneous coherence and condensation in the solid state, as will be discussed in the next section.

Fig. 1.3 shows a schematic of the band structure for indirect excitons. Note the

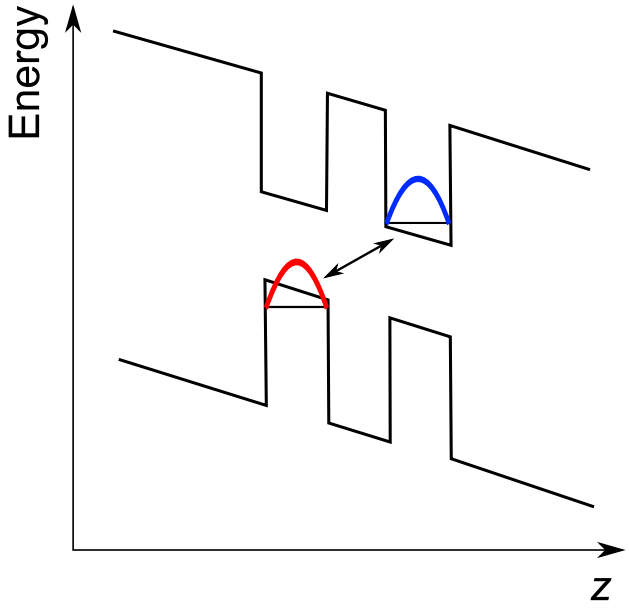

Figure 1.3: Energy diagram for a schematic coupled QW structure, where an electric field is applied in the z-direction, perpendicular to the QW planes.

fixed orientation of the exciton dipole (perpendicular to the plane of the QWs), which results in a repulsive interaction between excitons, favourable for BEC [20]. This repulsive interaction is also beneficial in preventing the formation of electron-hole droplets [21], and in resulting in effective screening of the disorder potential intrinsic to the structure [22]. Indirect excitons also have a larger Bohr radius and dipole moment, and the latter property is particularly important when considering interaction with electrons, since increasing the exciton dipole moment increases the exciton-electron interaction strength.

1.5 Condensation and coherence

One of the major driving forces in the study of excitons and polaritons in recent years has been the attempt to observe and understand macroscopic quantum phenomena in these complex solid-state systems [23, 14]. As mentioned earlier, excitons and polaritons in the low density regime behave as weakly interacting bosons, and hence may macroscopically occupy a single state, as occurs in a Bose-Einstein condensate (BEC). However, there is still much debate regarding the terminology of exciton and particularly polariton condensates [24, 25], and the differences compared to an equilibrium system such as a cold-atom BEC. This section will examine the generalities and specifics of condensation and coherent phenomena in excitonic systems.

1.5.1 Bose-Einstein condensation

The concept of BEC was first introduced as a phase transition in a system of non-interacting bosons. This was later extended for a system of weakly interacting bosons by Bogoliubov [26], and is now usually viewed in this context, since most of the interesting phenomenology arises as a result of interactions.

There are numerous definitions of BEC, all equivalent in the ideal case, however the central idea is that there is macroscopic occupation of a single particle state,

$$\chi_0(\mathbf{r}) = |\chi_0(\mathbf{r})|e^{i\theta} \ , \tag{1.4}$$

with an associated order parameter $\Psi(\mathbf{r}) = \sqrt{N_0}\chi_0(\mathbf{r})$, which is non-zero in the

BEC state, where N_0 is the condensate occupation number. The transition to BEC is a thermodynamic phase transition, occurring in a system with a defined temperature, and an example of spontaneous coherence, where long-range spatial coherence, or off-diagonal long range order [27, 28], is established at the transition, accompanied by the breaking of gauge symmetry.

The pure BEC state was first observed in trapped cold-atom gases at extremely low temperature [29, 30], as was demonstrated by interference measurements of initially separated BECs, which showed that the BECs exhibited spatial coherence across the entire condensate.

1.5.2 Superfluidity

Superfluidity is usually considered as the flow of a fluid without dissipation, or metastable flow. This example of spontaneous coherence was first observed in helium-4 in 1938 [31, 32]. The effect was quickly associated with BEC by F. London [33], and although helium-4 is a strongly interacting system, it is generally agreed that superfluidity occurs due to a finite fraction of the fluid being in a BEC state.

A clearer demonstration of superfluidity in, for example, helium-4 is the Hess-Fairbank effect [34], also known as nonclassical rotational inertia. The analogue of the Meissner effect in superconductivity [35], this is an equilibrium effect where the moment of inertia of a rotating fluid is decreased reversibly upon passing through the transition to superfluidity.

Landau was successfully able to describe superfluidity phenomenologically using a

two-fluid model, and without the assumption of BEC [36]; however superfluidity is generally understood as occurring due to the existence of phase coherent paths in the fluid, which follows from the definition of BEC. This can be seen in the equation for the superfluid velocity, below which a fluid may flow without dissipation:

$$v_{\mathrm{s}}(\mathbf{r}) = \frac{\hbar}{m}\nabla\theta(\mathbf{r}) \ , \tag{1.5}$$

where θ is the phase, as introduced in Eq. 1.4.

Landau's two-fluid model for superfluidity introduced two types of quasiparticle excitations in a superfluid: the phonon, a quantised sound wave, and the roton, which takes its name from the original idea that it corresponded to quantised rotational motion or vortices. These two quasiparticles correspond to different regions of the characteristic dispersion relation of elementary excitations, introduced phenomenologically by Landau. The idea of a roton was expanded by Feynman [37], and indeed in superfluid helium-4, a strongly interacting system, a roton minimum is observed [38]. The dispersion relation of the elementary excitations of superfluid helium was later reconstructed using neutron scattering data, and is plotted in Fig. 1.4. In 1946, Bogoliubov was able to derive the phonon-like part of the dispersion relation assumed by Landau, using a many-body theory and assuming BEC [26].

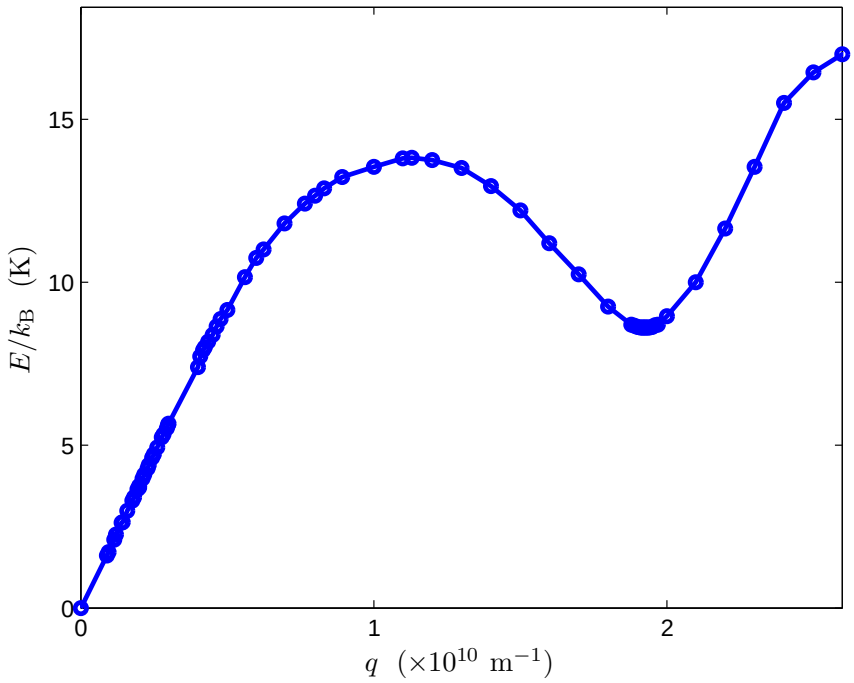

Figure 1.4: Dispersion of the elementary excitations of superfluid liquid helium, showing the linear phonon part at low wavevectors and the roton minimum at higher wavevector. Plotted using inelastic neutron scattering data from [39].

1.5.3 Two-dimensional excitonic systems

In general, the critical temperature for the transition to BEC satisfies

$$T_{\mathrm{c}} \sim \frac{n^{2/d}}{m} \ , \tag{1.6}$$

where d is the system dimensionality. It is therefore clear that the critical temperature for BEC may be greatly enhanced (or the critical density greatly reduced) for bosons such as excitons and polaritons, which have low mass compared to the mass of an atom.

An infinite and uniform 2D system of bosons of course does not have a BEC phase transition at finite temperatures in the thermodynamic limit [40, 41], however in trapped or finite systems the density of states is modified such that a BEC or quasi-BEC phase is recovered for finite temperature [42].

On the other hand, the Berezinsky-Kosterlitz-Thouless transition is a topological phase transition unique to 2D systems, which is driven by formation of vortices [43, 44]. It is thought that in a finite 2D system, both a BEC phase and a BKT phase should be present [45]. Both these phases display macroscopic phase coherence, however apart from the nature of the transition, the phases differ in the nature of coherence in the system - in the BKT phase there is a power law decay of the phase correlation function, while in the BEC phase there is instead long range order, where the first order spatial coherence tends to a finite value. It is expected that for the small system sizes in typical excitonic experiments a finite size BEC phase transition will occur at a higher temperature than the BKT transition [46].

The possibility of polaritons forming a condensate was first suggested in 1996 [47], in the form of a polariton laser, which would emit coherent light from a macroscopically occupied state, and which would have a very low threshold when compared to a conventional laser. Polariton lasing was indeed observed not long after in CdTe [11] and GaAs [48] based devices. Importantly, the effect has also even been demonstrated at room temperature in a GaN based device [49], in which the large exciton binding energy ensures stability of the exciton even at these high temperatures.

The question then asked was whether a BEC of polaritons could be observed in these systems, which are intrinsically nonequilibrium, with polariton decay due to imperfect light confinement balanced by pumping. A polariton laser does not require thermal equilibrium of the polaritons which occupy the ground state and form the condensate, and therefore BEC as a thermodynamic phase transition is not a sensible description in this case. Polariton lasers in general operate in the kinetic regime, in which the lifetime is short compared to the thermalisation time, and the polariton gas is therefore not in thermal equilibrium with a defined temperature [50]. There is however still macroscopic occupation of a coherent state, and the lack of equilibrium does not prevent observation of a high degree of spatial coherence in polariton condensates [51].

BEC of polaritons was first claimed in 2006 [52] and later in other systems up to room temperature [53, 54, 55], where it was shown that the polaritons could reach thermal equilibrium. The idea is then that since polaritons are in thermal equilibrium, the transition to a condensed state is thermodynamically driven and the condensate may be described by a steady state Bose-Einstein distribution

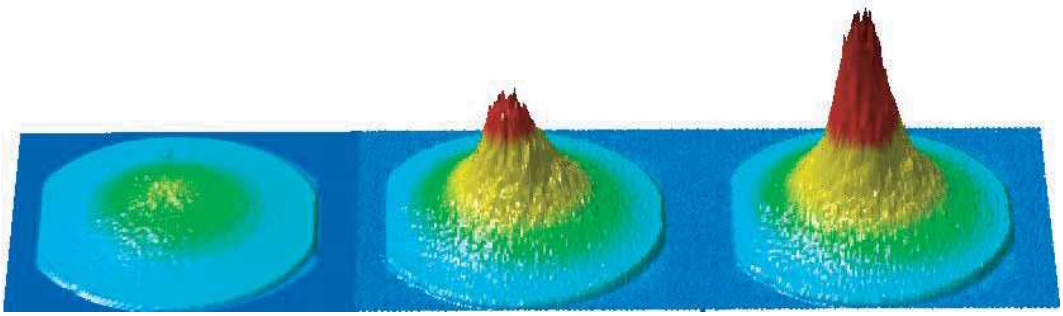

Figure 1.5: The sharp threshold observed in emission from the lower polariton ground state with increase in pumping power, as the condensate threshold is crossed - from [52].

peak, superimposed on a thermal Boltzmann distribution [56]. Fig. 1.5 shows the threshold in population of the lower polariton dispersion at zero in plane wavevector. For systems with a spin degree of freedom, such as excitons and polaritons, spontaneous coherence is also evidenced through the spontaneous buildup of the polarisation degree [57] - a spontaneous symmetry breaking in the system. This may be presented as evidence for a BEC phase transition, and was observed in 2008 [54].

However the polariton gas is not in thermal equilibrium with the lattice, or with the higher energy exciton states which coexist at the same spatial regions as the condensate. This presents a significant difference with the case of a cold-atom condensate, where the whole system has a single defined temperature. It is also argued that since the polariton condensate inherits its coherent properties from the photonic component, BEC is a misleading term for polariton condensates. Indeed, it has been shown that VCSELs exhibit many of the same coherent features as a polariton condensate, and that spontaneous symmetry breaking is even observed in the weak-coupling photon lasing regime of a microcavity [58]. The question of

whether BEC has been demonstrated in polariton systems is essentially a question of definition, and in this thesis the term polariton condensate refers simply to a macroscopically occupied coherent state of polaritons, disregarding the kinetics of formation, or other subtleties such as the degree of thermalisation. The nonequilibrium nature of polaritons, while complicating interpretation of experiment, also provides an opportunity to observe a multitude of interesting effects, such as pattern formation [59], and other phenomena associated with superfluidity discussed below.

Indirect excitons in coupled QW structures have also been shown to form a condensate state [60, 61, 62]. The long lifetime of these indirect excitons allows thermal equilibrium between the exciton gas and the lattice to be reached. It has been more difficult to show spontaneous coherence in indirect exciton systems than for a polariton system, due to heating sources and the influence of disorder in these systems, however recent experiments have shown that spontaneous coherence does indeed emerge at low temperatures [63]. Systems of dipoles display long range interactions and have been shown to exhibit a range of exotic phenomena [64]. The fixed dipole of the indirect exciton also enables simple control using electric fields, compared to the polariton, which has a very small dipole moment. Many interesting phenomena have been observed in cold exciton systems, such as the macroscopic order and pattern formation seen in Fig. 1.6.

Since the demonstration of condensation in exciton and polariton systems, much work has moved on to consider the transport properties in these systems. Polariton superfluidity has been claimed in a resonantly excited polariton condensate, evidenced by suppression of scattering from a defect [65, 66], while other interesting

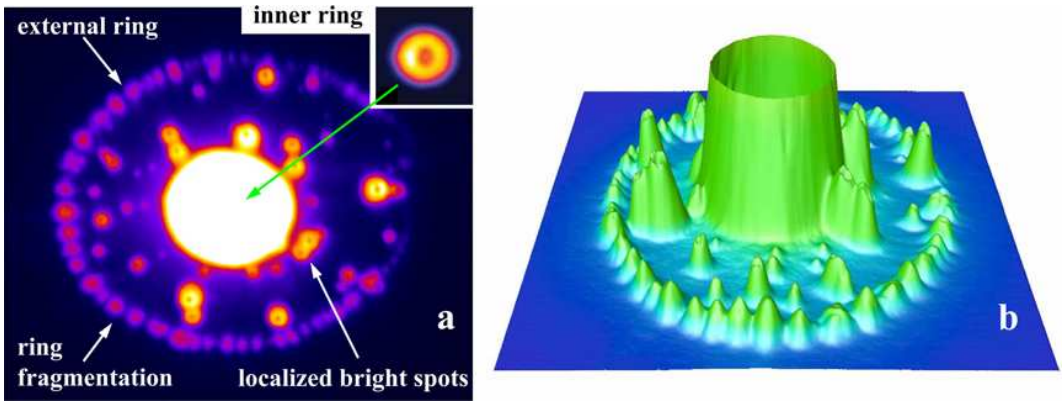

Figure 1.6: Images of the photoluminescence in (a) 2D and (b) 3D, of a coupled QW structure, showing pattern formation and the macroscopically ordered exciton state - from [23].

properties such as quantised vortices [67, 68], and linearisation of the dispersion relation [69] have also been observed. The question of whether these phenomena justify the term superfluidity can again be debated, emphasising the uniqueness of nonequilibrium polariton systems [70]. The variety and complexity of the phenomena demonstrated in these systems makes them an extremely interesting testing ground for nonequilibrium effects, and allows the observation of macroscopic quantum effects not possible in any other system, such as direct imaging of the macroscopic quantum wavefunction [71].

1.6 Hybrid Bose-Fermi systems

The ability to produce excitonic condensates has been widely demonstrated, and emphasis has moved on to the study of phenomena specific to these condensates, and the ways in which the advantages of excitonic systems may be exploited in applications. This in part mirrors the development of the cold-atom community,

where much research in recent years has studied applications, for example in quantum information, and more complex systems, such as Bose-Fermi mixtures [72].

The hybrid Bose-Fermi systems considered in this thesis are designed to allow interaction between fermionic and bosonic subsystems, which are however spatially separated. The fermionic subsystem consists of a gas of carriers trapped in a QW, a 2DEG, while the bosonic subsystem is a exciton or polariton condensate, confined in a separate QW or QWs. Systems containing both polaritons and free carriers have been previously studied, and shown to interact efficiently in order to assist polariton relaxation [73, 74].

The two subsystems may each exhibit different quantum effects as a result of their statistics. Both fermionic and bosonic systems may in some sense condense, and exhibit superfluid effects, implying superconductivity for charged fermions such as electrons. A bosonic system may also show further ordering, in a transition from a superfluid to a supersolid phase [75], an exotic crystalline yet superfluid phase, which may have been observed in liquid helium [76]. A system combining both a condensate and a 2DEG thus presents an extremely interesting solid-state laboratory in which one may investigate a variety of quantum effects - in principle even the superconducting and supersolid phases. The mutual interaction between the condensate and the filled Fermi sea of the 2DEG (the electron-exciton interaction) influences the behaviour within each subsystem, allowing further control of the parameters of the phase space, to reach regimes not possible in the absence of interaction.

1.6.1 Screening

In the remainder of this section, the relevant interactions within the systems studied will be considered in more detail. Firstly, to estimate the interaction between the different components in a Bose-Fermi system, one must consider how to account for the screening induced in systems of mobile charges, which acts to limit the range of the Coulomb interaction. The theory of screening in electronic systems is complex, and approximations are necessary in order to account for screening in a tractable way. Screening in a weakly interacting electron gas is normally accounted for by defining a wavevector and frequency dependent effective interaction

$$V_{\text{eff}}(\mathbf{q},\omega) = \frac{V(\mathbf{q})}{\epsilon(\mathbf{q},\omega)} \ , \tag{1.7}$$

where $V(\mathbf{q})$ is the bare Coulomb potential in Fourier space, and $\epsilon(\mathbf{q},\omega)$ is the dielectric response function obtained in the random-phase approximation. Additional approximations are then made where necessary in order to simplify the problem further.

The next sections study the interactions present in the systems of free carriers (electrons) and excitons, which are considered in this thesis. The aim is not to produce accurate quantitative predictions of the screened interactions in these systems, but to capture the approximate behaviour in a relatively simple way. For example, the effects due to mismatches in the dielectric constants of the different layers in the systems are neglected, which as a first approximation seems sensible. Other work has been published examining in detail the effect of this kind of mismatch in the systems considered here, and shows that neglecting this effect is

indeed a reasonable first approximation [77].

In this thesis, two interaction regimes will be distinguished within the systems considered. In the weak coupling regime, screening is accounted for within the component of interest, the electronic component, and a weak coupling theory is followed to calculate the effective electron-electron interaction, neglecting the effect of electrons on the condensate. However, it will also be shown later that increasing the Bose-Fermi interaction, coupling may induce qualitative changes to the condensate excitation spectrum, which requires a self-consistent treatment of the interactions between and within components.

1.6.2 Electron-electron interaction

The bare Coulomb potential in Fourier space for electrons in a 2DEG is given by [78]

$$V(\mathbf{q}) = \frac{e^2}{2\epsilon_{\mathrm{r}}\epsilon_0 A}\frac{1}{|\mathbf{q}|} \ , \tag{1.8}$$

where A is the sample area, and ϵ_{r} is the relative dielectric constant of the material. Screening in the 2DEG may then be accounted for by using Eq. 1.7. The full Lindhard dielectric function is often then simplified further by taking the static approximation ($\omega \to 0$), which for a 2DEG results in the Yukawa potential:

$$V_{\mathrm{C}}(\mathbf{q}) = \frac{e^2}{2\epsilon_{\mathrm{r}}\epsilon_0 A}\frac{1}{|\mathbf{q}| + \kappa} \ , \tag{1.9}$$

where κ is the two dimensional Thomas-Fermi screening wavevector [78], given by

$$\kappa = \frac{m_{\mathrm{e}} e^2}{2\pi\hbar^2 \epsilon_{\mathrm{r}} \epsilon_0}(1 - e^{-\pi\hbar^2 n_{\mathrm{e}}/m_{\mathrm{e}} k_{\mathrm{B}} T}) \ , \tag{1.10}$$

and n_{e}, m_{e} are the electron 2D concentration and effective mass, respectively.

1.6.3 Electron-exciton interaction

In the systems considered in this thesis, the 2DEG and excitonic condensate are spatially separated, located in QWs separated by a distance L. The exchange interaction is ruled out in general due to the difference in the effective masses of an electron in a 2DEG compared to an electron in an exciton, therefore only the direct interaction is considered.

The matrix element of the direct interaction between excitons and electrons reads:

$$V_{\mathrm{X}}(\mathbf{q}) = \int \Psi^*_{\mathrm{X}}(\mathbf{Q}, \mathbf{r}_e, \mathbf{r}_h)\Psi^*(\mathbf{k}, \mathbf{r}_1)V(\mathbf{r}_1, \mathbf{r}_e, \mathbf{r}_h)\Psi^*_{\mathrm{X}}(\mathbf{Q}, \mathbf{r}_e, \mathbf{r}_h)\Psi^*(\mathbf{k}, \mathbf{r}_1)d\mathbf{r}_1 d\mathbf{r}_e d\mathbf{r}_h \ , \tag{1.11}$$

where $\mathbf{r}_1, \mathbf{r}_e, \mathbf{r}_h$ correspond to the 2D coordinates of the 2DEG electron, the exciton electron and the exciton hole respectively. The 2DEG electron is described by a plane wave while the electrons and holes in the condensate are assumed to be in the $1s$ bound state with plane wave centre of mass motion:

$$\Psi(\mathbf{q}, \mathbf{r}_1) = \frac{1}{\sqrt{A}} e^{i\mathbf{k}\mathbf{r}_1} \ , \tag{1.12}$$

$$\Psi^*_{\mathrm{X}}(\mathbf{Q}, \mathbf{r}_e, \mathbf{r}_h) = \sqrt{\frac{2}{\pi A}} \frac{U_e\left(z_e\right) U_h\left(z_h\right)}{a_B} e^{i\mathbf{Q}\cdot\mathbf{R}_{\mathrm{X}}} e^{-r_{\mathrm{X}}/a_B} \ , \tag{1.13}$$

where $\mathbf{R}_{\mathrm{X}} = \beta_e \mathbf{r}_e + \beta_h \mathbf{r}_h$, $\mathbf{r}_{\mathrm{X}} = \mathbf{r}_e - \mathbf{r}_h$ are the in-plane coordinates of the centre of mass of the exciton, and the relative coordinate of electron and hole in the exciton. $U_e(z_e)$ and $U_h(z_h)$ are the normal to the QW plane electron and hole envelope functions, respectively. The exciton may also possess a dipole moment d, which can be intrinsic to the structure, because of spatial separation of electrons and holes in coupled QWs, or, in the case of microcavities, be induced by an internal piezo-electric field or an externally applied electric field. To account for all these possibilities, one can consider the layers of electrons and holes in the exciton shifted in the z-direction with respect to the position of the centre of mass by a distance $l = d/e$.

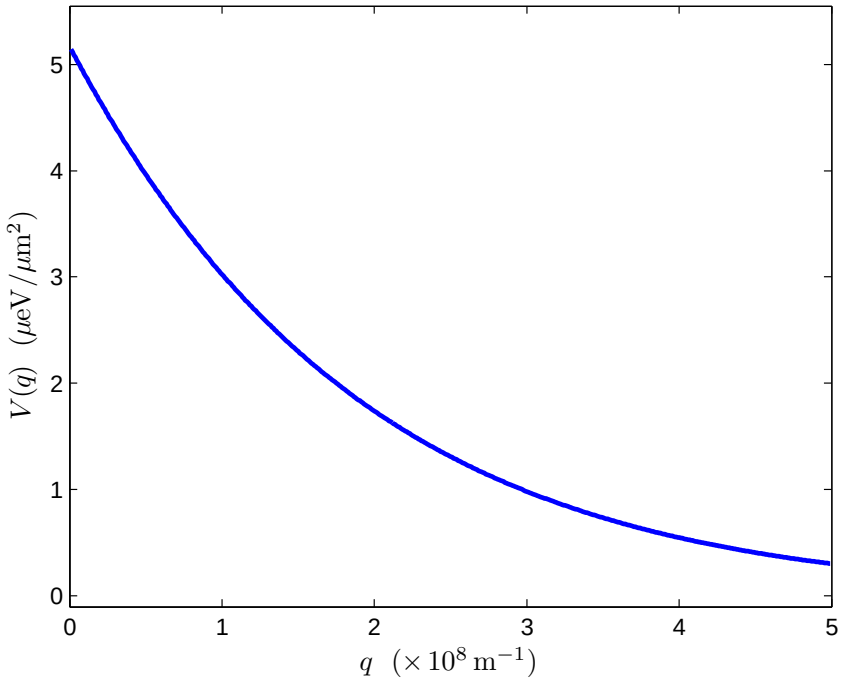

Figure 1.7: The exciton-electron interaction matrix element, normalised by the sample area. Parameters are taken as those realistic for a GaN-based system, while the exciton is assumed to have a dipole separation of 4 nm.

The exciton-electron matrix element, V_{X}, is then given by

$$V_{\mathrm{X}}(q) = \frac{ede^{-qL}}{2\epsilon_{\mathrm{r}}\epsilon_0 A}\left\{\frac{\beta_e}{\left[1+(\frac{\beta_e q a_B}{2})^2\right]^{3/2}}+\frac{\beta_h}{\left[1+(\frac{\beta_h q a_B}{2})^2\right]^{3/2}}\right\} + \frac{e^2e^{-qL}}{2\epsilon_{\mathrm{r}}\epsilon_0 qA}\left\{\frac{1}{\left[1+(\frac{\beta_e q a_B}{2})^2\right]^{3/2}}-\frac{1}{\left[1+(\frac{\beta_h q a_B}{2})^2\right]^{3/2}}\right\}, \tag{1.14}$$

where $\beta_{e,h} = m_{e,h}/(m_e + m_h)$, with $m_{e,h}$ being the effective masses of electrons and holes, and d being the dipole moment of the exciton in the normal to the QW plane direction. This potential is plotted in Fig. 1.7, which shows that the potential attains its maximum at zero exchanged momentum, due to the dipole interaction.

1.6.4 Exciton-exciton interaction

The exciton-exciton interaction is in general difficult to calculate [79], however an approximate expression may be derived assuming excitons are present in the system as an exciton or polariton condensate, and neglecting the wavevector and spin dependence of the interaction, as is widely done in the description of exciton and polariton condensates [80, 59, 81]. The dipole-dipole interaction is normally much smaller than the short ranged exchange interaction between excitons, and therefore is also neglected. Under these approximations the exciton-exciton interaction matrix element is given by [82]

$$U = \frac{6a_{\mathrm{B}}^2 E_{\mathrm{b}} X^4}{A}\ , \tag{1.15}$$

where E_{b} is the exciton binding energy. As mentioned earlier, this interaction is repulsive, which results in a linearisation of the excitation spectrum of the condensate.

Chapter 2

Vertical cavity surface emitting terahertz

In chapter one, microcavity systems were considered as both a laboratory for many interesting optical and condensed matter phenomena, and in terms of the possible applications, such as the polariton laser. In this chapter a novel and potentially important application of microcavity systems is presented, in which the system demonstrates terahertz (THz) lasing, in addition to polariton lasing from a macroscopically occupied polariton ground state [83].

In technological and scientific terms, coherent sources of THz radiation are highly sought after, due to the fact that THz radiation is non-ionising and able to penetrate a wide variety of non-conducting materials. The potential applications are diverse, and include use in industrial quality control [84], medical imaging [85], security [86] and spectroscopy [87]. However, the utilisation and development of applications of THz radiation has been severely limited by the difficulty of producing reliable, efficient, cheap, and compact THz sources, which sit at the interface between electronic devices able to generate lower frequency radiation, and opti-

cal devices operating at higher frequencies. The THz sources which are currently used, such as quantum cascade lasers [88, 89], cannot yet bridge all the difficulties to enable their widespread utilisation. A major fundamental problem for a device producing THz radiation is the long time for spontaneous THz emission, compared to the lifetime of the excitation. This may be enhanced by the Purcell effect, in devices where the emitter is enclosed within a THz cavity [90], however this enhancement also adds to the bulk, complexity and therefore cost of the device.

Recent work has proposed using microcavities to generate THz radiation, where the final state in a THz transition is a condensate of exciton-polaritons. In this system, bosonic stimulation of the transition may lead to enhancement of the THz emission [91, 92, 93]. The THz transition utilised is in this case the transition from the upper to the lower polariton branch, and would be accompanied by polariton lasing from the lower polariton branch.

However, this dipole transition is not optically allowed, since the upper and lower polaritons have the same parity, and therefore an electric field is required in order to hybridise the upper polariton with a different exciton state, such that the transition becomes allowed. This proposed system would operate in the waveguide geometry, which while confining THz radiation in the vertical direction perpendicular to the cavity, requires further confinement in the form of a lateral THz cavity to achieve emission in a single direction.

The alternative microcavity-based THz system studied here instead utilises an optically allowed transition from the $2p$ exciton state to the lowest energy polariton state, formed by the $1s$ exciton and cavity photon. The $2p$ exciton state cannot

be optically excited through absorption of a single photon, due to optical selection rules, however two-photon excitation of this state has already been demonstrated in GaAs quantum well structures [94, 95]. By pumping the $2p$ exciton state, radiative decay may then populate the lower polariton ground state, accompanied by the emission of THz photons at zero wavevector [96], and hence in a vertical direction. If this population is fast enough compared to the decay of lower polaritons, then a threshold to condensation may exist, leading to stimulation of the THz transition. This system is an improvement on the previous proposals due to the fact that the transition is optically allowed, in the vertical direction, and the whole structure is microscopic, with no need for a THz cavity. Recent work has studied the absorption of THz radiation by the lower polariton branch, showing that this indeed leads to the excitation of $2p$ excitons [97]. An interesting associated fundamental effect is also shown to occur in this system: the calculated threshold is dependent on the statistics of the pump used to populate the $2p$ exciton state.

2.1 System design

Fig. 2.1 shows a schematic of the system considered. As shown, the emission from the microcavity is perpendicular to the microcavity plane, in the vertical direction - as is the case in a vertical cavity surface emitting laser. The microcavity Bragg mirrors are transparent to THz radiation. No waveguides are needed and the THz transition is optically allowed, hence no additional electric field is necessary.

The $2p$ exciton state is excited by two-photon absorption, using a laser in the optical range, with frequency half that of the $2p$ exciton state. $2p$ excitons may then

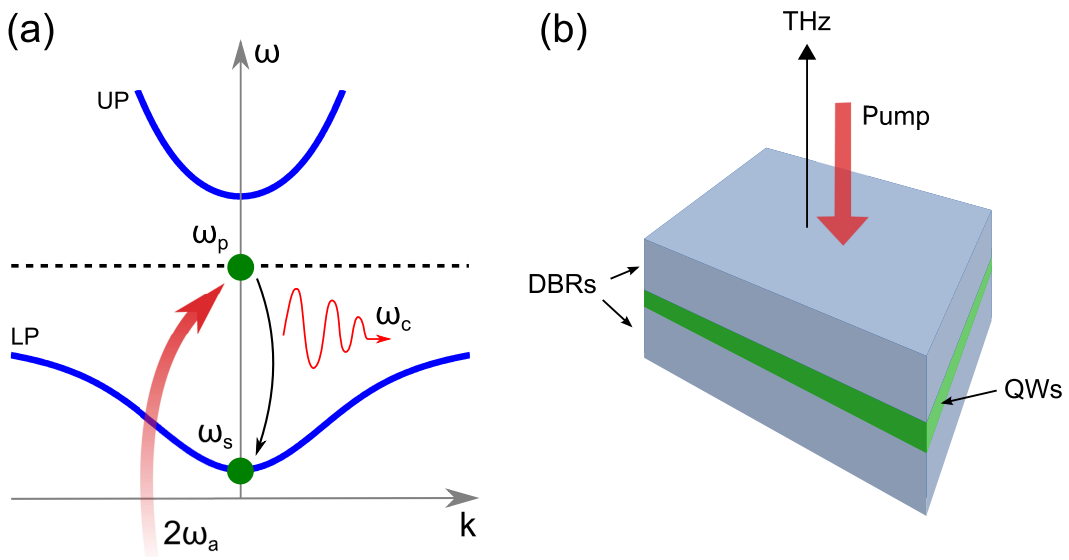

Figure 2.1: (a) Schematic of the polariton dispersion relation, showing the lower-polariton (LP) and upper-polariton (UP) branches, as well as the $2p$ exciton state with frequency ω_p. The pump frequency, ω_a, is half that of the $2p$ exciton state, as discussed in the text. (b) The structure considered in this work: a semiconductor microcavity consisting of an active layer containing quantum wells (QWs) sandwiched between two distributed Bragg reflectors (DBRs). The structure is pumped vertically, i.e. in the direction perpendicular to the microcavity plane, and the resulting THz emission from the cavity is in the same direction.

decay to the lower polariton branch, formed by the $1s$ exciton and cavity photon. This transition is accompanied by emission of a THz photon, and acts as a pump for the polariton ground state. If this process is efficient enough compared to the lower polariton lifetime, then the polariton ground state may become macroscopically occupied, leading to polariton lasing. This also has the effect of stimulating the THz transition to a macroscopically occupied bosonic final state, which results in a threshold behaviour in the $1s$ state population, and hence also in the THz emission from the microcavity (since, in the ideal case one THz photon would be emitted for each $1s$ polariton created, and hence also for each photon emitted by the polariton laser).

2.2 Quantum model

The laser is modelled by considering the density matrix describing the system, which is composed of the $2p$ exciton state, the lower polariton $1s$ ground state, and optical and THz photonic modes. It is assumed that the upper polariton state is significantly higher in energy than the $2p$ exciton state, and thus can be neglected.

The starting point is then the Liouville-von Neumann equation for the total density operator of the system,

$$i\hbar\frac{\partial\rho}{\partial t} = [H, \rho] \ , \tag{2.1}$$

where H is the total Hamiltonian of the system - comprising the $2p$ and $1s$ states and the classical reservoir, which in turn consists of the optical and THz photon modes.

The usual approximations are then applied in order to obtain the master equation in Lindblad form for the reduced density matrix. The Liouville-von Neumann equation is first converted into an integral over time, and a partial trace is taken over the reservoir R. The Born approximation is made, which assumes weak coupling between the subsystem and reservoir, and that the reservoir is therefore not affected by this interaction. This allows the total density matrix to be written as a product state, $\rho = \varrho \otimes \varrho_R$. Next the Markov approximation is made, which assumes the system has no memory (the system evolves slowly compared to the correlation time of the reservoir) and the final approximation is the rotating wave approximation, which restricts the transitions considered to those which conserve energy.

The equation for the reduced density matrix is then

$$\frac{d\varrho}{dt} = \frac{i}{\hbar}\left[\varrho, H_{\mathrm{c}}\right] + \mathcal{L}\varrho \ , \tag{2.2}$$

where now the Hamiltonian H_{c} simply describes the coherent evolution of the system, i.e. the free propagation and polariton-polariton interaction. Polariton-polariton interactions are neglected here since they simply result in a renormalisation of the condensate energy. The Lindblad superoperator $\mathcal{L}$ describes the dissipative excitation and relaxation processes, due to interaction of the quantum subsystem with the classical reservoir of photonic modes - the pump mode and the THz emission mode.

The Lindblad superoperator may be written in terms of the dissipative part of the

Hamiltonian, which can further be divided into two contributions:

$$H_d = \sum_i (H_i^+ + H_i^-) \ . \tag{2.3}$$

H_i^+ describes the creation of an excitation in the quantum subsystem (and thus annihilates an excitation in the classical reservoir), while H_i^- governs the reverse process. The subscript index i numerates the different dissipative processes in the system.

The Lindblad superoperator can therefore be written as [98, 99]

$$\begin{aligned}\mathcal{L}\varrho = \frac{\delta(\Delta E)}{\hbar} \sum_i \big\{ & 2\left(H_i^+ \rho H_i^- + H_i^- \varrho H_i^+\right) \\ & - \left(H_i^+ H_i^- + H_i^- H_i^+\right)\varrho - \varrho\left(H_i^+ H_i^- + H_i^- H_i^+\right)\big\} \ ,\end{aligned} \tag{2.4}$$

where $\delta(\Delta E)$ accounts for energy conservation, and in realistic calculations should be taken as an average inverse broadening of the states in the system, $\delta(\Delta E) = \zeta^{-1}$. In the particular system considered here, the terms contributing to the dissipative part of the Hamiltonian can be written as

$$H_1^+ = g p^\dagger a^2 \ , \tag{2.5}$$

$$H_1^- = g p (a^\dagger)^2 \ , \tag{2.6}$$

$$H_2^+ = G p^\dagger s c \ , \tag{2.7}$$

$$H_2^- = G p s^\dagger c^\dagger \ , \tag{2.8}$$

where p and s denote annihilation operators of the $2p$ exciton and the lowest energy

$1s$ polariton states, respectively, a is the annihilation operator for laser photons exciting the $2p$ exciton state, and c is an annihilation operator for THz photons produced by the $2p \rightarrow 1s$ transition. The constants g and G define the strengths of the two-photon excitation of the $2p$ state and $1s \rightarrow 2p$ THz transitions, respectively. Phonon assisted relaxation of the $2p$ exciton to the $1s$ state is neglected, since this process is forbidden due to orbital momentum conservation.

For a density operator which obeys Eq. 2.2, one can evaluate the evolution of the average value of an arbitrary operator $\langle A \rangle = \mathrm{Tr}(\varrho A)$, using $\partial_t \langle A \rangle = \mathrm{Tr}(\partial_t \varrho A)$. The coherent part does not contribute to the kinetics, so that

$$\begin{aligned} \partial_t \langle A \rangle &= \frac{1}{\hbar\zeta}[\mathrm{Tr}(\varrho[H^-;[A;H^+]]) + \mathrm{Tr}(\varrho[H^+;[A;H^-]])] \ , \\ &= \frac{2}{\hbar\zeta}\mathrm{ReTr}(\varrho[H^-;[A;H^+]]) \ . \end{aligned} \tag{2.9}$$

In order to obtain rate equations for the occupancies of the $2p$ and $1s$ states, the substitutions $A = p^\dagger p$ or $A = s^\dagger s$ are made, giving

$$\begin{aligned} \frac{dN_p}{dt} &= Tr\left\{p^\dagger p \frac{d\varrho}{dt}\right\} = \frac{2}{\hbar\zeta}\mathrm{Re}\{\mathrm{Tr}\left(\varrho[H^-;[p^\dagger p;H^+]]\right)\} \ , \\ &= W_g\left[\frac{1}{2}\langle (a^\dagger)^2 a^2\rangle - \langle p^\dagger p(2a^\dagger a + 1)\rangle\right] \\ &\quad + W_G\left[\langle s^\dagger s c^\dagger c\rangle - \langle p^\dagger p(s^\dagger s + c^\dagger c + 1)\rangle\right] \ , \end{aligned} \tag{2.10}$$

where $W_g = 4g^2/\hbar\zeta$ and $W_G = 2G^2/\hbar\zeta$. The equation for the polariton mode occupancy $N_s = \langle s^+ s\rangle$, is analogous to that for N_p, and the occupancy of the pumping mode $N_a = \langle a^+ a\rangle$ is simply defined by the intensity of the external pump.

To simplify these equations, a mean field approximation is made, so that the fourth-order correlators may be factorised into products of second order correlators. For example $\langle p^{+}pa^{+}a\rangle \approx \langle p^{+}p\rangle\langle a^{+}a\rangle = N_pN_a$. However, the correlator $\langle a^{+2}a^2\rangle$ may be written in terms of the second order coherence function as

$$\langle a^{+2}a^2\rangle = g^{(2)}(0)N_a^2 \ . \tag{2.11}$$

The THz mode occupancy, is taken as $N_{\rm c} = 0$, since there is no confinement of the THz mode. Therefore the equations of motion for the occupation numbers of the $2p$ and $1s$ states read

$$\frac{dN_p}{dt} = -\frac{N_p}{\tau_p} + W_g\left[\frac{g^{(2)}(0)}{2}N_a^2 - N_p(2N_a+1)\right] - W_GN_p\left(N_s+1\right) \ , \tag{2.12}$$

$$\frac{dN_s}{dt} = -\frac{N_s}{\tau_s} + W_GN_p\left(N_s+1\right) \ , \tag{2.13}$$

where the possibility of decay of $2p$ excitons through non-radiative processes is included, with an associated lifetime τ_p. The (radiative) lifetime of the $1s$ state is also added, and is denoted $\tau_{\rm s}$.

Perhaps surprising is the dependence of the $2p$ state population on the second order coherence function of the exciting light. For a coherent laser pump, the statistics are Poissonian and $g^{(2)}(0) = 1$, however in the case of a thermal pump, $g^{(2)}(0) = 2$. The dependence of two-photon optical processes on the second order coherence of light has been previously discussed by Ivchenko [100].

The time dependent solutions may be obtained through the use of a standard solver in MATLAB, however in order to demonstrate a threshold behaviour one

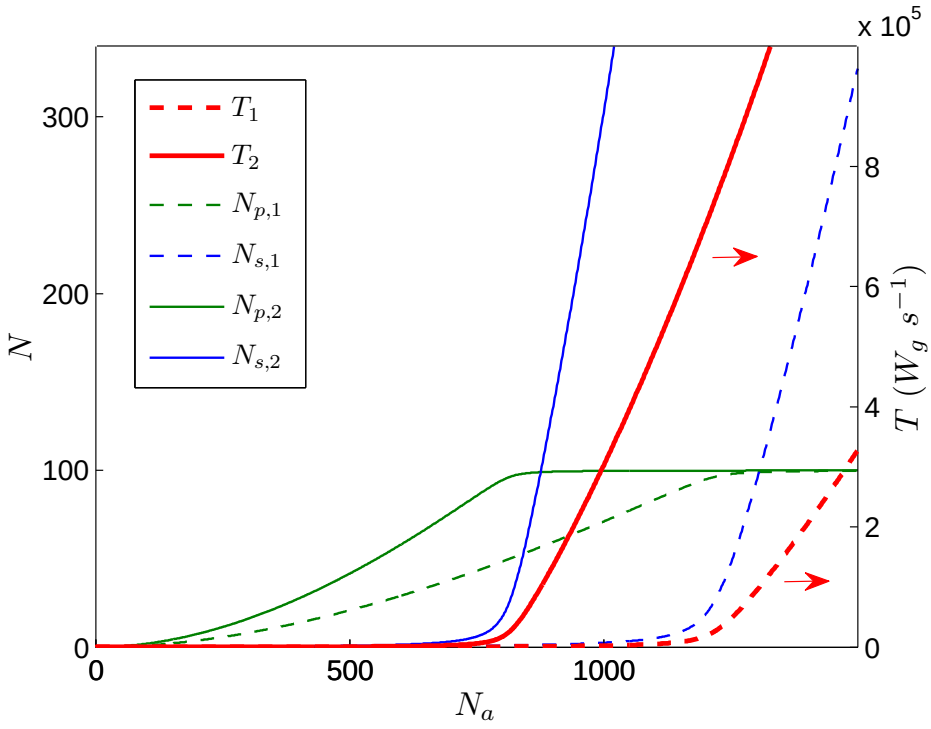

Figure 2.2: Occupation of the p- and s-states (left axis) and terahertz generation rate (right axis) in the steady state, as a function of pumping mode occupancy. The subscript 1 or 2 refers to the value of $g^{(2)}(0)$ taken. $W_g = 1, W_G = 10, 1/\tau_s = 1000, 1/\tau_p = 5000$, in units of W_g.

need only consider the steady state for a given pumping power. The steady state solutions for the $2p$ and $1s$ state occupations are easily obtained through solution of a quadratic equation for N_p and are plotted in Fig. 2.2. A threshold behaviour can be observed in the $1s$ state occupation with increasing pumping power, and hence also in the THz emission rate, which is proportional to the s-state occupation. The occupations are plotted for the different photon statistics mentioned above, and show that the pumping threshold is higher for a coherent pump. This can be understood as being due to stimulated two-photon emission, which enhances losses from the $2p$ state.

The threshold occurs when the $2p$ state population is large enough, in order that transitions to the $1s$ state are in balance with its losses due to finite lifetime. Once the occupation of the $1s$ state is of order one, the THz transition is stimulated, leading to a rapid buildup of the population and accompanying THz emission. The criterion $N_s \sim 1$, is satisfied when $N_p \sim 1/W_G\tau_s$, and hence the terahertz generation rate is given by

$$T = W_G N_p(N_s + 1) = \frac{N_s}{\tau_s} \ , \tag{2.14}$$

and therefore shows the same threshold behaviour with pumping intensity as N_s, as can also be seen in Fig. 2.2. This threshold to THz lasing occurs with the threshold to polariton lasing, for which the emission is in the optical range. Therefore the emission from the polariton laser may act as a visible signal of the THz generation.

2.3 Summary

In this chapter, a proposal has been presented for a microcavity THz laser, which emits in the vertical direction from a microscopic cavity and therefore could be easily scaled in power output (by tiling a series of microcavities). The frequency of THz emission could be tuned by altering the detuning between the exciton resonance and the photonic mode of the microcavity, which is usually done by varying the cavity width with position, in wedged structures. The laser would also have a very low threshold, given by the threshold of the microcavity to polariton lasing, while in the ideal case the microcavity would emit a single THZ photon for every optical photon, allowing high efficiencies to be achieved. The use of GaN- or ZnO-based microcavities would even allow room temperature operation, a significant advantage in terms of the potential for general application.

The system has been modelled using a master equation approach to derive the equations of motion for the relevant state occupations. A threshold to THz lasing has been shown to exist, and interestingly this threshold is predicted to be sensitive to the statistics of the pump.

My contribution to the work presented in this chapter consisted of working on the derivation of the rate equations using the master equation approach, solving the rate equations generally and in the steady state, and generating the presented figures.

Chapter 3

Light mediated superconductivity

Superconductivity is an extraordinary example of an effect of the quantum world manifested at macroscopic scales, being equivalent to a superfluid of charged bosons, with a macroscopic order parameter associated with their condensation. The most obvious effect of the phase transition to superconductivity is the complete loss of electrical resistance, and hence the ability of the material to act as a perfect conductor. However a superconductor is not simply a perfect conductor, and it is the Meissner effect, the expulsion of magnetic field from the interior as the phase transition is crossed, i.e. perfect diamagnetism, which is usually taken to characterise the superconducting state.

As a macroscopic quantum phenomenon, superconductivity usually requires low temperatures, so that the thermal energy does not dominate over the other energy scales in the system. However, there have been sustained and intense efforts towards extending this quantum effect to higher and higher temperatures. Until relatively recently, it was believed that an upper limit for observation of superconductivity existed at around 30 K, however the discovery of cuprate superconductivity [101] showed that conventional superconductivity was only a subset of that

which could occur. This discovery was extremely interesting from the fundamental point of view, as it quickly became clear that BCS theory could not adequately describe this new class of superconductors. It was also a great leap forward for the application of superconductivity, which could now be observed in systems cooled using liquid nitrogen, rather than costly and difficult liquid helium. Cuprate superconductivity generated huge excitement due to the idea that materials may even exist in which the phase transition occurred above room temperature. However, the further extension to higher temperatures has not occurred, and a theoretical description of the high temperature superconductors is still lacking. Indeed, theoretical and experimental work on superconductivity has split into numerous branches, with significant current research on heavy-fermion [102], cuprate [103], organic [104] and iron-based [105] materials, as well as work attempting to find completely new systems in which superconductivity may be observed. It is within this final branch that the work presented in this chapter resides.

In this chapter, a hybrid Bose-Fermi system is studied; the system is designed in order to modify the electron-electron interaction such that formation of Cooper pairs and superconductivity may occur. The Bose-Fermi coupling is assumed to be weak, and the system is described using BCS theory, with a bosonic exciton or polariton condensate mediating the electron-electron interaction. The excitations of this condensate are then analogous to the phonons which mediate the electronic pairing interaction in conventional low temperature superconductors. In the first section, the history of superconductivity will be discussed, describing the construction of the microscopic BCS theory, which was successfully applied to describe conventional phonon mediated superconductivity. The most obvious

generalisation in the application of this theory is to relax the assumption of the phonon as the mediating boson. BCS theory will then be applied to the specifics of the system studied here, demonstrating the possibility of high critical temperatures in exciton and polariton systems.

3.1 The theory of superconductivity up to 1957

Superconductivity was famously first observed by H. K. Onnes in 1911, in experiments studying the electrical resistance of mercury at low temperatures [106]. In 1933 the Meissner effect was observed [107] - an equilibrium effect perhaps more surprising than the abrupt loss of resistance observed by Onnes - where a weak magnetic field is expelled from a superconducting material as it passes through the superconducting transition. This perfect diamagnetism is not simply the behaviour that would be expected of a perfect conductor, which would exclude magnetic field in the superconducting state, but which would actually trap any field present on passing from the normal to superconducting state.

The experimental observation of superconductivity came well before the theoretical tools existed to explain the microscopic mechanism. The collective nature of superconductivity required the application of many-body quantum mechanics, while in the early years after the discovery of superconductivity, quantum mechanics was not a well understood theoretical framework.

The first phenomenological theory of superconductivity was constructed by the brothers F. and H. London and published in 1935 [108]. They began with the assumption that electrons in a superconductor accelerate uniformly in response to an

electric field, i.e. the existence of a supercurrent. From this they derived a second equation relating the supercurrent density to the magnetic field in a superconductor, which successfully yields the Meissner effect. The London theory predicts a penetration depth of a magnetic field into the bulk of a superconductor, however this was shown to underestimate real penetration depths. This led Pippard to generalise the London equations by assuming that the current response was non-local, i.e. depended on the field over a finite volume, with a radius representing the spatial extent of the superconducting wavefunction, the coherence length [109].

F. London later stated the idea that superconductivity was an example of a macroscopic quantum state, however, theorists struggled to apply quantum mechanics to superconductivity as a collective many-body effect. It was also not until 1950 that theoretical work was able to phenomenologically describe the macroscopic properties of the superconducting state. This theory was constructed by Ginzburg and Landau [110], and was based on Landau's theory of second order phase transitions, which states that there is a complex order parameter describing the ordering, or loss of symmetry, upon moving across a phase transition of this type. The order parameter is zero in the normal state, and increases continuously into the ordered state. Expressing the free energy in terms of this order parameter and minimising with respect to its variation leads to the Ginzburg-Landau equations, which contain information about the form of the order parameter. It was later shown that Ginzburg-Landau theory is actually a limiting form of the full microscopic BCS theory, valid close to T_c [111]. This leads to the interpretation of the order parameter as a macroscopic wavefunction of condensed Cooper pairs.

A highly significant experimental discovery was made in 1950 with work demon-

strating the dependence of the superconducting critical temperature on the isotope, and hence on the nuclear mass [112, 113]. This was a clear indication of the role of the lattice in superconductivity, or the role of interaction of electrons with phonons in a quantum mechanical picture, and an important step towards a sought-after microscopic theory of superconductivity. The isotope effect was implicitly predicted in a work of H. Fröhlich, in which a Hamiltonian for the electron-phonon interaction was constructed [114].

The phenomenological Ginzburg-Landau theory is an extremely successful and useful theory for studying the macroscopic properties of superconductors, however it should strictly only be applied close to the critical temperature, and it was not clear what the order parameter corresponded to physically. The phenomenological theory also depended on a number of parameters, which could not be determined from first principles, and is not applicable for length scales less than the coherence length, as Pippard's work demonstrated. For these reasons and in order to understand the origins of superconductivity, a microscopic theory was a major goal for many of the top theorists working in condensed matter.

3.2 BCS theory

The breakthrough came in 1957 with the publication of the microscopic Bardeen-Cooper-Schrieffer theory, or BCS theory [115, 116]. Many of the ingredients of the theory had been developed over the preceding years, such as the existence of an energy gap of order $k_{\mathrm{B}}T_{\mathrm{c}}$ between the ground state and the excited states of the superconductor, widely assumed theoretically, and shown to exist by measurement

of the exponential dependence of the specific heat below the transition [117].

By the mid-1950s, progress had been made in understanding the outline of a possible mechanism of superconductivity. Building on work by Fröhlich [118], Bardeen was able to show how an attractive interaction between electrons might arise. This work was carried out with D. Pines, and resulted in the so-called Bardeen-Pines potential, which provides a model effective interaction between electrons close to the Fermi surface, mediated by phonons, which is attractive provided the energy exchanged is small [119]:

$$V(q,\omega) = \frac{e^2}{\epsilon_0(q^2+\kappa^2)}\left(1+\frac{\omega_q^2}{\omega^2-\omega_q^2}\right) , \tag{3.1}$$

where κ denotes the Thomas-Fermi screening wavenumber, q is the exchanged (phonon) wavenumber, $\hbar\omega$ the exchanged (phonon) energy, and $\hbar\omega_{\mathrm{q}}$ the phonon dispersion.

The mathematics of the many-body theory was still out of reach, however significant progress was made in 1956, when Cooper was able to show the existence of an instability for pairs of electrons close to the Fermi surface, on top of a filled Fermi sea [120]. Cooper considered a pair of electrons in time-reversed momentum states: a spin-singlet pair state, for electrons with equal and opposite momenta. He showed that for a pair close to the Fermi surface, a bound state exists at an energy lower than the filled Fermi sea, for an arbitrarily small attractive interaction. This is despite the fact that the kinetic energy of electrons ($\sim E_F$) is much larger than the binding energy. The instability can be understood naively by considering that electrons on top of a filled Fermi sea may only scatter to states in

a quasi-two-dimensional shell, due to the Pauli principle; there is then a general result which says that in two dimensions, a bound state exists for any attractive interaction [121].

The remaining problem was to account for the collective nature of the superconducting state; knowing that there exists an instability for a single electron pair, it is not clear how this leads to the macroscopic occupation of a new ground state. The calculation of Cooper provided a clue, since it showed that the instability occurred only between pairs with conjugate momenta; BCS therefore incorporated this into the effective model Hamiltonian.

The BCS Hamiltonian may be derived using a Fröhlich transformation of the electron-phonon Hamiltonian, which eliminates the first order electron-phonon coupling [118]. The model Hamiltonian is given by

$$H_{\mathrm{BCS}} = \sum_{\mathbf{k},\sigma} \xi_k c^\dagger_{\mathbf{k}\sigma} c_{\mathbf{k}\sigma} + \sum_{\mathbf{k},\mathbf{k}'} V_{\mathbf{k}\mathbf{k}'} c^\dagger_{\mathbf{k}\uparrow} c^\dagger_{-\mathbf{k}\downarrow} c_{-\mathbf{k}'\downarrow} c_{\mathbf{k}'\uparrow} \ , \tag{3.2}$$

where $\xi_k = \varepsilon_k - \mu$, $\varepsilon_k = \hbar^2 k^2 / 2m^*$, and μ is the chemical potential. $c^\dagger_{\mathbf{k}\sigma}$, $c_{\mathbf{k}\sigma}$ are second quantised electron creation and annihilation operators respectively, obeying the usual fermionic anticommutation relations. $V_{\mathbf{k}\mathbf{k}'}$ is the potential between pairs with initial momenta $\mathbf{k}'$,$-\mathbf{k}'$ and final momenta $\mathbf{k}$,$-\mathbf{k}$. The second summation is restricted to states within an energy $\hbar\omega_{\mathrm{D}}$ of the Fermi surface, where ω_{D} is the Debye frequency, which defines the cutoff in the phonon spectrum.

The successful solution begins with an ansatz for the superconducting ground

state, as devised by Schrieffer:

$$|\Psi_{\mathrm{BCS}}\rangle = \prod_{\mathbf{k}} (u_{\mathbf{k}} + v_{\mathbf{k}} c^{\dagger}_{\mathbf{k}\uparrow} c^{\dagger}_{-\mathbf{k}\downarrow})|0\rangle \ , \tag{3.3}$$

where $u_{\mathbf{k}}, v_{\mathbf{k}}$ are parameters, satisfying the normalisation condition $u^2_{\mathbf{k}} + v^2_{\mathbf{k}} = 1$, and $|0\rangle$ is the filled Fermi sea. This coherent ground state is not an eigenstate of the number operator, i.e. it is not number conserving (since phase and number are conjugate variables). The method of solution is equivalent to a mean field approach, where the average value of the number is fixed, but not the number itself - hence the system is in the grand canonical ensemble and energy is measured relative to the chemical potential. A mean field approach turns out to be extremely accurate, due to the large size of Cooper pairs compared to the inter-electron spacing, and therefore their highly overlapping nature.

In order to determine the parameters $u_{\mathbf{k}}$ and $v_{\mathbf{k}}$, BCS used a variational approach, minimising the expectation value of the Hamiltonian in the ground state. This leads to the following self-consistency condition, the gap equation:

$$\Delta_{\mathbf{k}} = -\sum_{\mathbf{k}'} V_{\mathbf{k}\mathbf{k}'} \frac{\Delta_{\mathbf{k}'}}{2E'_{\mathbf{k}}} \ , \tag{3.4}$$

where $\Delta_{\mathbf{k}}$ is the gap function, and $E_{\mathbf{k}} = \sqrt{\xi^2_{\mathbf{k}} + \Delta^2_{\mathbf{k}}}$ is the quasiparticle excitation energy, with the characteristic gap which leads to superconductivity. As already mentioned, the gap function can be shown to be equal to the order parameter in the Ginzburg-Landau theory of superconductivity, aside from a numerical factor.

To simplify the problem further, BCS then used the following model potential:

$$V_{\mathbf{k}\mathbf{k}'} = \begin{cases} -V & \text{if } |\xi_{\mathbf{k}}|, |\xi'_{\mathbf{k}}| < \omega_{\mathrm{D}} \ , \\ 0 & \text{otherwise} \ , \end{cases} \tag{3.5}$$

which is justified by Cooper's work showing that the phonon mediated interaction may be attractive over a certain frequency range, with a cutoff given by the cutoff in the phonon spectrum. For this choice of potential, the gap equation, Eq. 3.4, is satisfied for a gap function which is equal to a constant where the potential is negative, and zero otherwise. Hence the gap equation may be simplified to

$$1 = \frac{V}{2} \sum_{\mathbf{k}} \frac{1}{E_{\mathbf{k}}} \ . \tag{3.6}$$

Replacing the momentum sum by an integral over energy gives

$$1 = \mathcal{N}V \int_0^{\hbar\omega_{\mathrm{D}}} \frac{d\xi}{\sqrt{\Delta^2 + \xi^2}} = \mathcal{N}V \sinh^{-1}\left(\frac{\hbar\omega_{\mathrm{D}}}{\Delta}\right) \ , \tag{3.7}$$

where $\mathcal{N}$ is the density of states at the Fermi surface, in the normal state. Then assuming weak coupling, $\mathcal{N}V \ll 1$, gives

$$\Delta \approx 2\hbar\omega_{\mathrm{D}} e^{-1/\mathcal{N}V} \ . \tag{3.8}$$

For finite temperatures, the gap equation may be generalised using the Fermi function $f(E_{\mathbf{k}}) = (e^{E_{\mathbf{k}}/k_{\mathrm{B}}T} + 1)^{-1}$:

$$\Delta(\xi, T) = -\int_{-\infty}^{\infty} \frac{U(\xi - \xi')\Delta(\xi', T)\tanh(E/2k_{\mathrm{B}}T)}{2E} \, d\xi' \ , \tag{3.9}$$

where $U(\xi) = \mathcal{N}V(\xi)$ is now a general arbitrary dimensionless potential. The critical temperature T_c can then be determined as the temperature at which the gap function at zero energy goes to zero. For the BCS potential this gives

$$k_B T_c = 1.13\hbar\omega_D e^{-1/\mathcal{N}V} \ . \tag{3.10}$$

Shortly after, Bogoliubov published an alternative approach [122], convenient for studying the excitations of the system, in which the Hamiltonian is diagonalised using a so-called Bogoliubov transformation, where the quasiparticle excited states (known as bogolons in general) are a combination of electron and hole states.

In summary, the BCS mechanism shows that superconductivity arises due to the existence of a new ground state, a coherent many-body state of Cooper pairs, which in some sense condense. These pairs are not strictly bosons, due to their highly overlapping nature, however the BCS state is a state of ODLRO of Cooper pairs, hence the interpretation of superconductivity as superfluidity of charged Cooper pairs. The physical picture for this mechanism in conventional superconductors is roughly as follows: an electron, moving in the lattice of ions in a metal, induces a distortion in the ion positions, due to the attractive Coulomb interaction. The response of the lattice is slow compared to the motion of the electron, due to the difference in mass, hence at a later time when the electron has moved a large distance away, the induced polarisation is still present and able to cause attraction of a second electron. This process creates an effective attractive interaction, for electron pairs which are separated by a large distance (or time), and therefore do not experience direct Coulomb repulsion - this is described as a retarded interaction

due to the time delay in the effective interaction. However the interaction at short times is still repulsive, limiting the critical temperature [123].

3.3 Exciton mediated superconductivity

BCS theory was extremely successful in explaining superconductivity in the conventional superconductors, where the phonon mediates the pairing interaction between electrons. However the BCS mechanism does not assume a particular form for the pairing interaction, only that it is attractive for pairs of electrons close to the Fermi surface. Considering Eq. 3.10, it is clear that the critical temperature in this case could be increased by increasing either the prefactor, or the denominator of the exponent. In this scheme (with a BCS-like potential), this means increasing the energy range over which an attractive interaction exists, increasing the strength of the attractive interaction V, or increasing the density of states at the Fermi surface, $\mathcal{N}$.

The existence of an alternative mechanism of superconductivity, where pairing is mediated by excitons, was first proposed by Little [124], and then extended by Ginzburg [125] and Allender, Bray and Bardeen [126], who considered layered metal-insulator structures. The idea was that the critical temperature could be raised due to an increase in the effective cutoff of the attractive pairing interaction, orders of magnitude greater compared to the phonon case. Attraction between electrons would occur via creation and annihilation of virtual excitations of the insulating semiconductor layer. However the probability of creating virtual excitons in the semiconductor layer is very low due to the large energy cost, and excitonic

superconductivity was never observed. The recent progress in demonstration of condensation in the solid-state, allows instead the consideration of systems of *real* excitons, and an attractive electron pairing interaction due to the presence of an excitonic condensate.

3.4 Condensates and superconductivity

The ability to produce excitonic condensates allows one to consider designing systems in which the attractive electron-electron interaction occurs not through interaction of electrons with the lattice, but instead through interaction with a condensate, where the condensate excitations replace phonons as the mediating boson. This may then even allow engineering of the electron pairing interaction, such that the phase transition to superconductivity occurs at a high temperature.

The first system considered is a microcavity system in which the electron-electron interaction is modified due to the presence of a polariton condensate in the lower polariton ground state. In this structure, schematically illustrated in Fig. 3.1, a single n-doped QW containing a 2DEG is sandwiched between two undoped QWs, where a polariton condensate is formed. These QWs are embedded in a microcavity, at a maximum of the confined light field, ensuring stability of the polariton condensate up to high temperatures (for example up to room temperature in a GaN microcavity, as reported in [55]). The delocalised nature of microcavity polaritons means that the excitons from both QWs are part of a single condensate, surrounding the 2DEG and maximising the interaction of the condensate with it. This allows higher densities of polaritons to be generated in the system while

remaining in the strong coupling regime; indeed the density could be increased further by repeating this basic unit. However, the necessity of continuous pumping in order to maintain the polariton population is a disadvantage of this system, due to the heating caused by the pump.

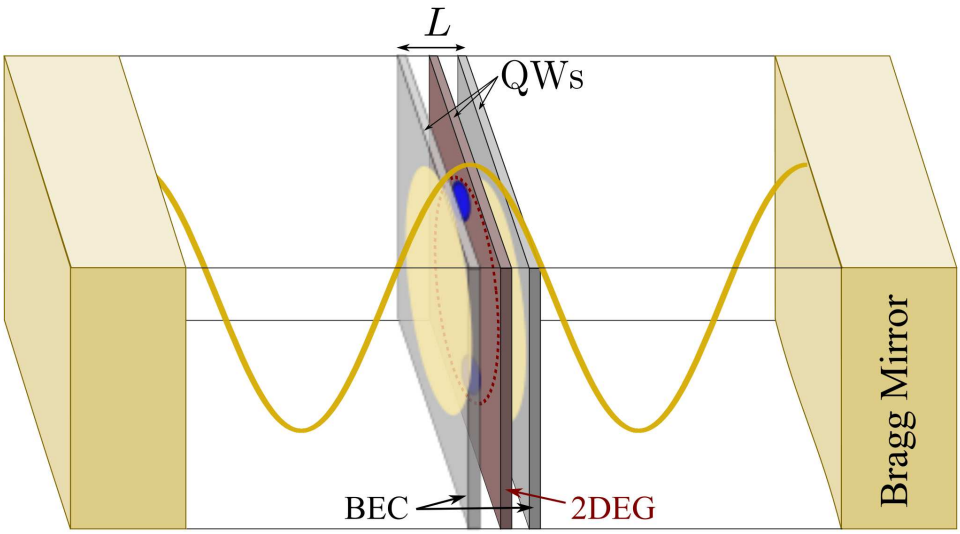

Figure 3.1: The model microcavity structure considered, with an n-doped QW surrounded by two undoped QWs where a polariton condensate is formed.

A simpler system may also be considered, in which there is no microcavity, but instead the 2DEG is placed in close proximity to a coupled QW structure, where indirect excitons are excited. This requires low temperatures in order to maintain a condensate, however an advantage of this system is that indirect excitons have an effectively fixed dipole moment, which enhances the interaction with electrons. The two cases are very similar, and one may switch between them simply by changing the dispersion relation and the Hopfield coefficient X, which is equal to one in the case of indirect excitons, and $1/\sqrt{2}$ for the polariton system. The square

of the Hopfield coefficient gives the excitonic fraction.

The Hamiltonian for the systems which are studied in this chapter is given by [127]

$$H = \sum_{\mathbf{k}} \left[E_{\mathrm{el}}(\mathbf{k}) \sigma_{\mathbf{k}}^{\dagger} \sigma_{\mathbf{k}} + E_{\mathrm{ex}}(\mathbf{k}) a_{\mathbf{k}}^{\dagger} a_{\mathbf{k}} \right] + \sum_{\mathbf{k}_1, \mathbf{k}_2, \mathbf{q}} \Big[V_{\mathrm{C}}(\mathbf{q}) \sigma_{\mathbf{k}_1+\mathbf{q}}^{\dagger} \sigma_{\mathbf{k}_2-\mathbf{q}}^{\dagger} \sigma_{\mathbf{k}_1} \sigma_{\mathbf{k}_2} + X^2 V_{\mathrm{X}}(\mathbf{q}) \sigma_{\mathbf{k}_1}^{\dagger} \sigma_{\mathbf{k}_1+\mathbf{q}} a_{\mathbf{k}_2+\mathbf{q}}^{\dagger} a_{\mathbf{k}_2} + U a_{\mathbf{k}_1}^{\dagger} a_{\mathbf{k}_2+\mathbf{q}}^{\dagger} a_{\mathbf{k}_1+\mathbf{q}} a_{\mathbf{k}_2} \Big] . \quad (3.11)$$

The electronic annihilation operators are denoted $\sigma_{\mathbf{k}}$ and the excitonic $a_{\mathbf{k}}$, while $E_{\mathrm{el}}(\mathbf{k})$ and $E_{\mathrm{ex}}(\mathbf{k})$ denote the in-plane dispersion relations of electrons and excitons (or polaritons), respectively. V_{C}, V_{X} are the electron-electron and electron-exciton interaction matrix elements, respectively, and U is the exciton-exciton (or polariton-polariton) interaction matrix element.

3.4.1 Effective interaction

In BCS theory, the repulsive Coulomb interaction between electrons is not included, due to Cooper's work showing that the ground state is unstable to formation of Cooper pairs for an arbitrarily small attractive interaction, and previous work by Fröhlich, and Bardeen and Pines, showing that the second order phonon mediated attraction can overcome the direct repulsion, due to the retardation effect. Their starting point was therefore the assumption of this attractive interaction for the pairs of electrons considered by Cooper. In this work however, it is necessary to demonstrate that the second order interaction mediated by the condensate is able to overcome the repulsive interaction; therefore the direct screened Coulomb interaction, given by Eq. 1.9, is included.

For the electron-exciton interaction matrix element, Eq. 1.14 is used. The screening between these two components - due mainly to the barrier layer(s) separating the condensate from the 2DEG - is therefore neglected. The exciton-exciton (or polariton-polariton) matrix element is given by Eq. 1.15.

BCS theory is followed, by transforming the Hamiltonian of the system into the form of the BCS Hamiltonian, Eq. 3.2, resulting in an effective interaction potential for pairs of electrons [127]. The first step is to make a mean field approximation for the excitonic part of the Hamiltonian, where the existence of a condensate is assumed, with occupation number N_0, so that for example $a^\dagger_{\mathbf{k+q}} a_{\mathbf{k}} \approx \langle a^\dagger_{\mathbf{k+q}} \rangle a_{\mathbf{k}} + a^\dagger_{\mathbf{k+q}} \langle a_{\mathbf{k}} \rangle$, and $\langle a_{\mathbf{k}} \rangle \approx \sqrt{N_0 A}\delta_{\mathbf{k},\mathbf{0}}$.

The condensate part is then in a biquadratic form so may be diagonalised using a Bogoliubov transformation:

$$a_{\mathbf{k}} = u_{\mathbf{k}} b_{\mathbf{k}} - v_{\mathbf{k}} b^\dagger_{-\mathbf{k}} \quad ; \quad a^\dagger_{-\mathbf{k}} = u_{\mathbf{k}} b^\dagger_{-\mathbf{k}} - v_{\mathbf{k}} b_{\mathbf{k}} \ , \tag{3.12}$$

where $b_{\mathbf{k}}$ are annihilation operators of the elementary excitations of the system (bogolons). The resulting Hamiltonian is very similar in structure to the electron-phonon Hamiltonian, where phonons have been replaced by bogolons, the elementary quasiparticle excitations of the condensate:

$$H = H_{\mathrm{el}} + \sum_{\mathbf{k}} E_{\mathrm{bog}}(\mathbf{k})\, b^\dagger_{\mathbf{k}} b_{\mathbf{k}} + \sum_{\mathbf{k},\mathbf{q}} M(\mathbf{q})\, \sigma^\dagger_{\mathbf{k}} \sigma_{\mathbf{k+q}} \left(b^\dagger_{-\mathbf{q}} + b_{\mathbf{q}} \right), \tag{3.13}$$

where H_{el} denotes the unchanged terms describing propagation and direct inter-

action of electrons. $E_{\rm bog}\left(\mathbf{k}\right)$ denotes the bogolon dispersion, given by

$$E_{\rm bog}(\mathbf{k}) = \sqrt{\tilde{E}_{\rm ex}(\mathbf{k})(\tilde{E}_{\rm ex}(\mathbf{k}) + 2UN_0A)}\ , \tag{3.14}$$

where $\tilde{E}_{\rm ex}(\mathbf{k}) \equiv E_{\rm ex}(\mathbf{k}) - E_{\rm ex}(\mathbf{0})$. $M\left(\mathbf{q}\right)$ is the renormalised bogolon-electron interaction strength, given by

$$M(\mathbf{q}) = \sqrt{N_0A}X^2V_{\rm X}(\mathbf{q})\sqrt{\frac{E_{\rm bog}(\mathbf{q}) - \tilde{E}_{\rm ex}(\mathbf{q})}{2UN_0A - E_{\rm bog}(\mathbf{q}) + \tilde{E}_{\rm ex}(\mathbf{q})}}\ . \tag{3.15}$$

The Hamiltonian Eq. 3.13 can be expressed as $H = H_0 + H_{\rm M}$, where $H_0 = H_{\rm el} + \sum_{\mathbf{k}} E_{\rm bog}\left(\mathbf{k}\right) b^\dagger_{\mathbf{k}} b_{\mathbf{k}}$ and $H_{\rm M} = \sum_{\mathbf{k},\mathbf{q}} M\left(\mathbf{q}\right) \sigma^\dagger_{\mathbf{k}} \sigma_{\mathbf{k}+\mathbf{q}} \left(b^\dagger_{-\mathbf{q}} + b_{\mathbf{q}}\right)$. Then a unitary Fröhlich transformation is made:

$$H' = e^{-S} H e^{S} = H + [H,S] + \frac{1}{2}[[H,S],S] + \dots\ , \tag{3.16}$$

where S is determined perturbatively in order to satisfy $H_{\rm M} + [H_0, S] = 0$, and hence eliminate the first order electron-bogolon coupling. The transformed Hamiltonian is given by

$$\begin{aligned} H' &\approx H_0 + \frac{1}{2}[H_{\rm M}, S] \\ &= H_0 + \sum_{\mathbf{k}_1,\mathbf{k}_2,\mathbf{q}} V_{\rm A}\left(\mathbf{q},\omega\right) \sigma^\dagger_{\mathbf{k}_1} \sigma_{\mathbf{k}_1+\mathbf{q}} \sigma^\dagger_{\mathbf{k}_2+\mathbf{q}} \sigma_{\mathbf{k}_2}\ , \end{aligned} \tag{3.17}$$

and an effective electron Hamiltonian may finally be written:

$$H_{\rm eff} = \sum_{\mathbf{k}} E_{\rm el}\left(\mathbf{k}\right) \sigma^\dagger_{\mathbf{k}} \sigma_{\mathbf{k}} + \sum_{\mathbf{k}_1,\mathbf{k}_2,\mathbf{q}} V_{\rm eff}\left(\mathbf{q},\omega\right) \sigma^\dagger_{\mathbf{k}_1} \sigma_{\mathbf{k}_1+\mathbf{q}} \sigma^\dagger_{\mathbf{k}_2+\mathbf{q}} \sigma_{\mathbf{k}_2}\ , \tag{3.18}$$

where $V_{\text{eff}}(\mathbf{q},\omega) = V_{\text{C}}(\mathbf{q}) + V_{\text{A}}(\mathbf{q},\omega)$, and

$$V_{\text{A}}(\mathbf{q},\omega) = \frac{2M(\mathbf{q})^2 E_{\text{bog}}(\mathbf{q})}{(\hbar\omega)^2 - E_{\text{bog}}(\mathbf{q})^2} \ . \tag{3.19}$$

This equation agrees with similar expressions obtained in the study of a Bose-Fermi mixture of atomic gases [128, 129].

The effective electron-electron potential is composed of the repulsive Coulomb part, and the (sometimes) attractive bogolon-mediated part. Importantly, the condensate induced attraction between electrons, V_{A} increases linearly with the condensate occupation, N_0, which is directly linked to the pumping power. Hence the attractive pairing interaction, and therefore the BCS gap, is optically controlled, which is a significant advantage over earlier proposals for exciton-mediated superconductivity. The attractive part of the effective interaction, V_{A}, is plotted in Fig. 3.3 as a function of wavevector for fixed frequency. The parameters used throughout this chapter are collected in Appendix A.

The wavevector dependence is then removed by taking an average over the Fermi surface:

$$U_0(\omega) = \bar{V}_{\text{A}}(\omega) + \bar{V}_{\text{C}} = \frac{A\mathcal{N}}{2\pi}\int_0^{2\pi} \left[V_A(q,\omega) + V_C(q)\right] d\theta. \tag{3.20}$$

where $\mathcal{N} = m_{\text{e}}/\pi\hbar^2$ is the energy density of states of the 2DEG at the Fermi surface. This average over the 2D Fermi surface is depicted in Fig. 3.2, and is taken in order to follow the approach used in BCS theory, where wavevector dependence is not taken into account since the interaction is assumed to be isotropic. Note that U_0 is a dimensionless quantity, due to the density of states factor. It is assumed that the potential depends only on the magnitude of the wavevector, and in this

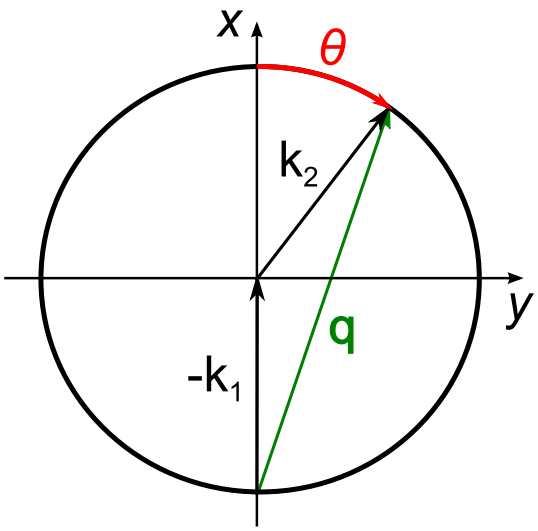

Figure 3.2: Fermi surface average in two dimensions. The vector $\mathbf{q} = \mathbf{k}_1 - \mathbf{k}_2$ is the exchanged wavevector between the interacting electron pair, and hence is equal to the phonon wavevector. $\mathbf{k}_1, \mathbf{k}_2$ are the initial and final wavevectors of the scattered electron, which both lie on the Fermi surface.

case the Fermi surface average is equivalent to that found by fixing one wavevector (say in the negative x-direction), and letting the other vary over the whole surface.

In two dimensions the average of the Coulomb part V_{C} may be calculated analytically, giving

$$\bar{V}_{\mathrm{C}} = \frac{\mathcal{N}e^2}{2\pi\epsilon_{\mathrm{r}}\epsilon_0} \frac{\pi - 2\arctan\left(\frac{2k_{\mathrm{F}}}{\sqrt{\kappa^2 - 4k_{\mathrm{F}}^2}}\right)}{\sqrt{\kappa^2 - 4k_{\mathrm{F}}^2}}\,, \tag{3.21}$$

where the substitution $q^2 = 2k_{\mathrm{F}}^2(1 + \cos\theta)$ has been made (see Fig. 3.2) and then the average performed over θ. The temperature dependence of the screening wavevector κ is neglected, which is a good approximation for large 2DEG densities. $\bar{V}_{\mathrm{C}}$ is then simply a dimensionless positive constant.

While the average of the Coulomb part may be calculated analytically, the average of $V_{\mathrm{A}}(q, \omega)$ must be found numerically, which necessitates dealing with the poles

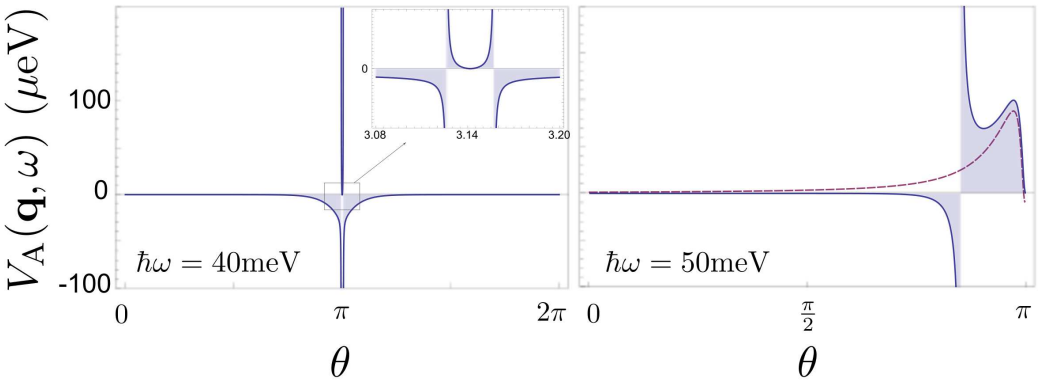

Figure 3.3: Effective electron-electron potential as a function of θ for two different energies (where $q^2 = 2k_F^2(1+\cos\theta)$). The potential is symmetric about $\theta = \pi$, as may be seen in the left-hand plot, where the inset shows the existence of two poles. For small energies, the potential is attractive over a wide range of θ, while repulsion dominates with increasing energy. The smoothed potential with no poles is shown as a purple dashed line in the right-hand plot.

where $(\hbar\omega)^2 = E_{\rm bog}(\mathbf{q})^2$, for each ω. These poles are of first order, and may therefore be removed analytically, leaving a smoothed integrand to be easily integrated numerically. This is done by defining

$$f(\theta) = (\theta - \theta_0)V_{\rm A}(\mathbf{q}(\theta),\omega) \ , \tag{3.22}$$

so that

$$\bar{V}_{\rm A} = \frac{A\mathcal{N}}{2\pi}\left[\int_0^{2\pi} \frac{f(\theta)-f(\theta_0)}{\theta-\theta_0}\,d\theta + f(\theta_0)\ln\frac{2\pi-\theta_0}{\theta_0}\right] \ , \tag{3.23}$$

where $f(\theta_0) = \lim_{\theta\to\theta_0} f(\theta)$. The argument of the integrand is now a smoothed function without poles, as is shown in Fig. 3.3 for example, while the second term comes from a simple analytical integration of the leftover term $f(\theta_0)/(\theta-\theta_0)$.

Fig. 3.4 shows this averaged potential, U_0, for the microcavity system, for differ-

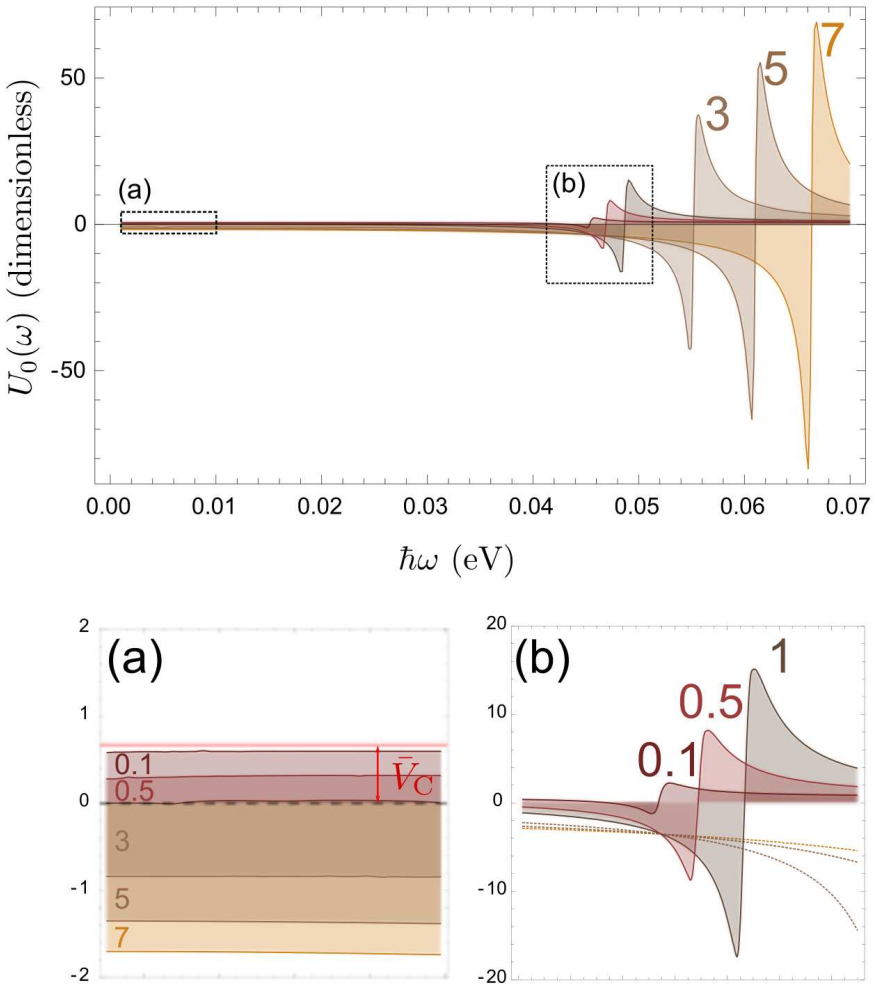

Figure 3.4: The effective electron-electron interaction potential U_0 for different values of the condensate density, which is indicated on the plots in units of 10^{12} cm^{-2}. The potential is attractive when the density of the condensate is high enough to overcome Coulomb repulsion, leading to Cooper pairing in the 2DEG. The Coulomb repulsion $\bar{V}_C$ is shown as a red line in (a).

ent values of the condensate density. For large enough densities, the potential is attractive over a range of frequencies from zero, corresponding to long time scales. The peculiar shape of the potential is due to the shape of the polariton potential.

In Fig. 3.5, U_0 is plotted for the case of an exciton condensate. In this case, the potential is more similar to a simple well, as taken by BCS. Compared to the potential for the microcavity system, it is more attractive at long time scales, however the attraction exists over a smaller energy range. As in the polariton case, the potential becomes repulsive at high frequencies, corresponding to short time scales.

3.4.2 The gap equation

Having obtained the dimensionless effective electron-electron potential, the gap equation must be next be solved:

$$\Delta(\xi, T) = -\int_{-\infty}^{\infty} \frac{U_0(\xi - \xi')\,\Delta(\xi', T)\tanh\left(E(\xi')/2k_BT\right)}{2E(\xi')}\,d\xi' \,. \tag{3.24}$$

This equation must be solved iteratively for the gap function, for a number of temperatures, in order to determine the critical temperature for superconductivity, T_c. With the approximation of a constant well for the potential, the gap equation is easily solved, as was seen earlier, however for a general potential, finding the solution is more difficult, and constituted the bulk of the work required in order to calculate critical temperatures. The gap equation was solved using MATLAB and exploiting the fact that the gap equation is equivalent to a convolution of the potential U_0 with the gap function normalised by the temperature dependent part

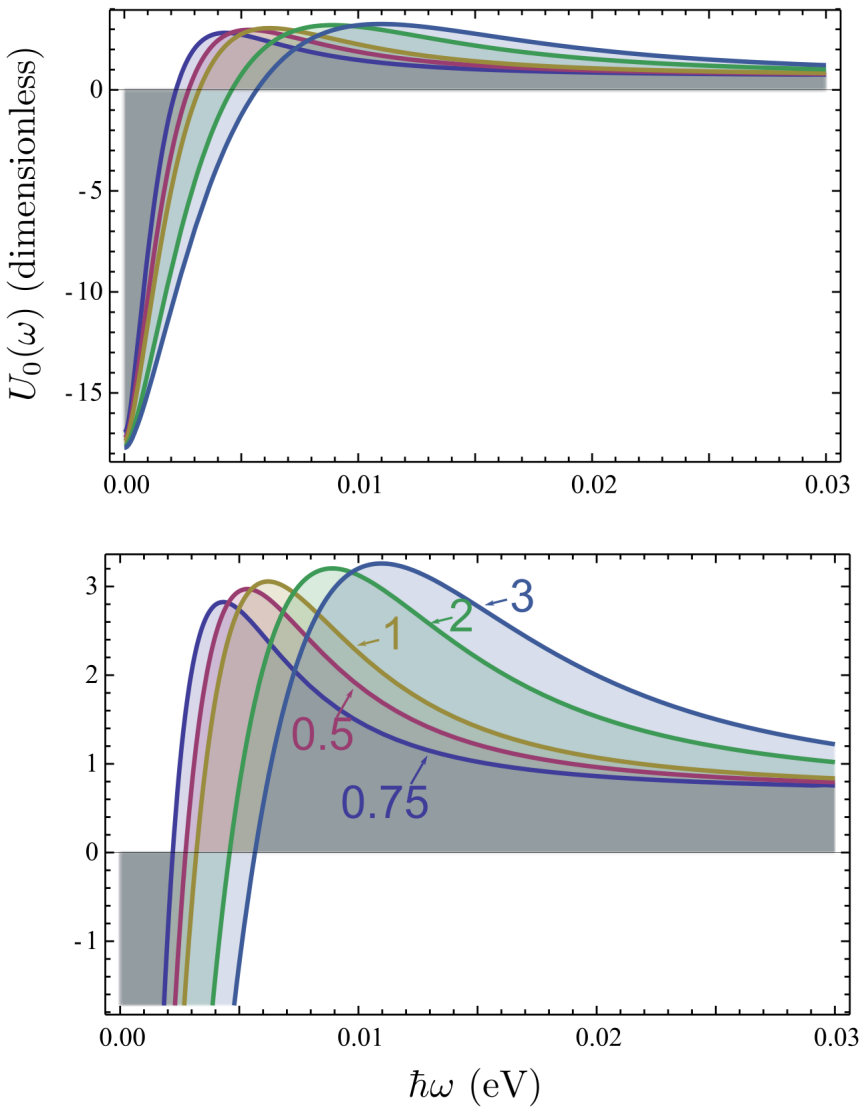

Figure 3.5: The effective electron-electron interaction potential U_0 for the case of an exciton condensate. In the lower plot, a zoom of the upper plot is shown. The densities are labelled as in Fig. 3.4.

and the quasiparticle energy. Each iteration of the gap function can therefore be computed relatively quickly using an inbuilt convolution function.

The gap equation is a non-linear integral equation, an example of a Hammerstein integral,

$$\Delta(\xi, T) = \int K(\xi, \xi') f[\xi', \Delta(\xi')]\, d\xi' \ . \tag{3.25}$$

It has been shown that for a wholly negative (attractive) potential, a unique and non-zero solution exists [130, 131], however the existence of a unique solution in the case of a potential which is repulsive for some values of its argument has not been demonstrated mathematically [132]. A solution may be found by substituting an initial value for the gap function in the right hand side of the equation (for example equal to a positive constant), and using this to calculate the left hand side, which is taken as the input for the next iteration. Using this method it can be shown that the BCS approximation is actually a very good approximation, when compared to the numerical solution [133].

However, for a general potential with repulsive regions as well as attraction, one cannot be sure that this method will converge to give a unique physical solution. Indeed the numerical solutions often exhibited instabilities for certain parameter ranges, with the solution having discontinuities in temperature for example. Therefore an approximate analytical solution is desirable, in order to compare to the numerical results.

3.4.3 Bogoliubov potential

An approximate solution may be found for step-valued potentials, such as a model potential known as the Bogoliubov potential [134, 135], which introduces repulsive regions either side of the attractive region in the BCS potential, as shown in Fig. 3.6. For this type of potential, the gap equation can be linearised by assuming the gap function is also a stepped function, to produce an approximate analytical solution for the critical temperature [133]:

$$k_{\mathrm{B}}T_{\mathrm{c}} \approx 1.13\hbar\omega_{\mathrm{D}} \exp\left(-\left(V_0 - \frac{V_{\mathrm{C}}}{1+\mathcal{I}V_{\mathrm{C}}}\right)^{-1}\right) , \tag{3.26}$$

where $\mathcal{I} = \ln(\omega_{\mathrm{C}}/\omega_{\mathrm{D}})$. Comparing this equation to Eq. 3.10, it is clear that the addition of repulsive regions introduces a correction to the BCS case, which however tends to zero with V_{C}. Numerical calculation of the gap function shows that the approximation as a stepped function is reasonable, when compared to the BCS approximation.

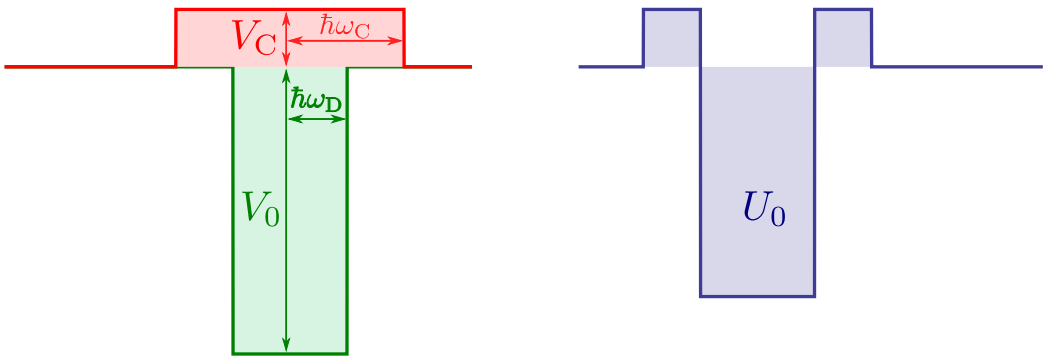

Figure 3.6: The model potential known as the Bogoliubov potential, where repulsion is introduced on top of the BCS potential.

Numerical solution of the gap equation gives the gap function as a function of

energy, for a fixed temperature. Therefore the critical temperature may be found by constructing the full temperature dependence of the gap function - obtained by solving the gap equation iteratively for number of different temperatures - to find the temperature at which the gap becomes equal to zero. However the convergence of the iterative method slows as the critical temperature is approached, a general phenomena known as critical slowing down. Therefore while it is relatively easy to calculate the gap function at zero temperature, it is much more computationally intensive to reconstruct the whole temperature dependence, in order to find the critical temperature. An approximate solution using the Bogoliubov potential is then useful as a quick method for calculation of T_{c}, and may be compared qualitatively to the gap function at zero temperature.

In BCS theory there is a linear relationship between the critical temperature and the gap at zero temperature, given by the universal relation

$$\frac{2|\Delta(0,0)|}{k_{\mathrm{B}}T_{\mathrm{c}}} = 3.53 \ . \tag{3.27}$$

This is a weak coupling result, and the ratio increases with an increase in coupling, up to a maximum of 4, where BCS theory is no longer applicable and the Eliashberg equations must instead be solved [136]. The relation is obtained assuming a BCS potential, and therefore a constant gap function, so is not directly applicable to this case, however there should nevertheless be an analogous relationship, allowing qualitative comparison of the two quantities. This is useful, since in some cases iteration of the gap equation does not converge to give a unique, well-behaved numerical solution. However, in most cases the solution does indeed converge, and demonstrates the same trends as the approximate calculation of T_{c} [133]. This

supports the use of this numerical solution, and the solutions found for parameters which do lead to convergence.

For the system containing an exciton condensate, an appropriately constructed Bogoliubov potential may be used to find an approximate value for the critical temperature. For the polariton potentials, the method may be extended, constructing a three-step potential [133].

3.4.4 Excitonic potential

Fig. 3.7 shows an example of the gap function calculated numerically for the microcavity system, exhibiting the same qualitative temperature dependence as the gap function calculated with the BCS potential. Calculation of a series of critical temperatures in this manner allows the demonstration of increasing critical temperature with density.

Numerically calculated critical temperatures for exciton and polariton systems are shown in Fig. 3.8. It can be seen that the critical temperature is strongly dependent on the condensate density, and increases to very high temperatures. These critical temperatures are not realistic since the condensate will collapse once strong coupling is lost, and since approximations have been made assuming a relatively low temperature. However, these calculations demonstrate that the mechanism is robust and extremely promising as a system for realisation of high temperature superconductivity, and for demonstration of superconductivity in a novel system.

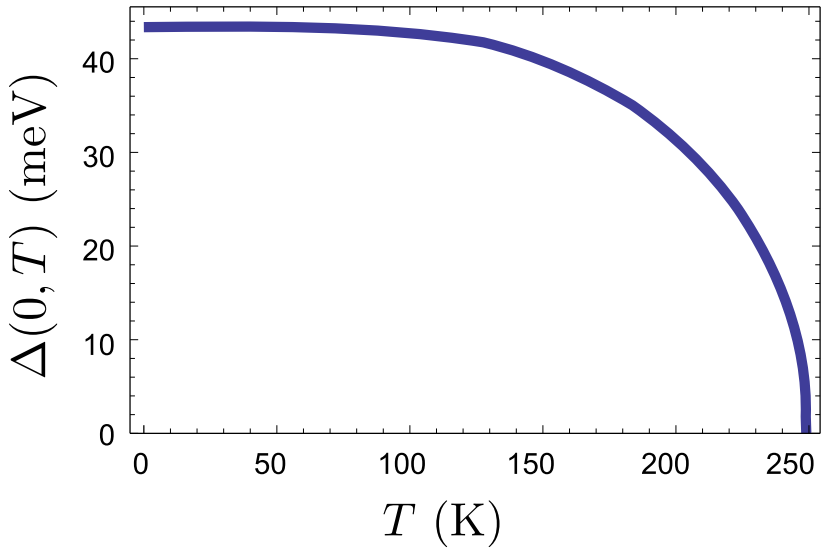

Figure 3.7: The gap function at zero energy calculated numerically, as a function of temperature, for a density $N_0 = 1.75 \times 10^{12}$ cm^{-2}. Parameters are those relevant to the microcavity case.

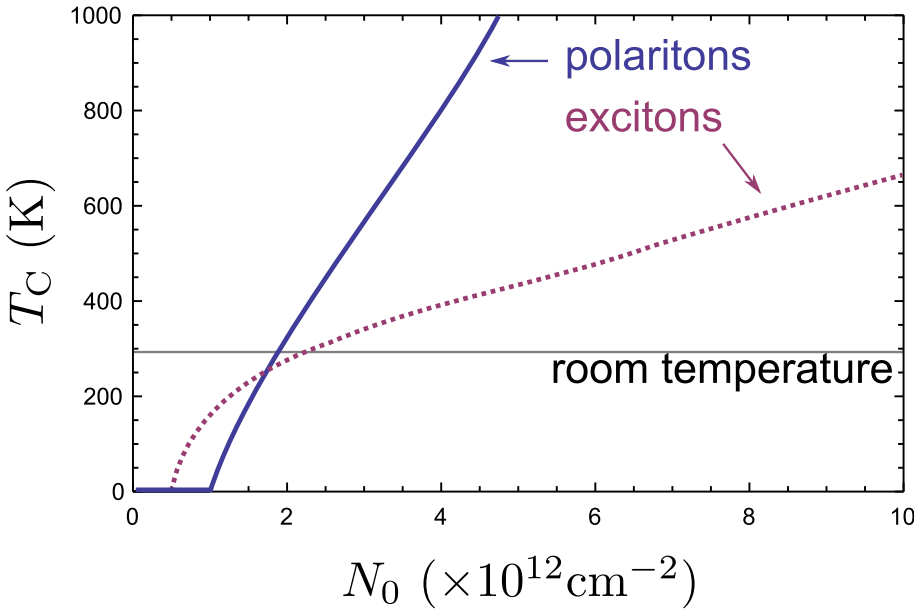

Figure 3.8: The critical temperature of superconductivity as a function of the condensate density.

3.5 Summary

In this chapter, BCS theory has been applied to a model of non-conventional superconductivity in which the electron pairing interaction arises due to the interaction of a 2DEG with an exciton or polariton condensate. It has been shown that the presence of a condensate may lead to effective attraction and pairing of electrons, and therefore superconductivity in the solid-state system, with enhanced critical temperatures which may even extend to above room temperatures in microcavity systems.

The main assumption made in this work is that the application of BCS theory is valid, i.e. that the coupling between the two subsystems is weak enough to be described using the mean field BCS theory, a single parameter theory which does not account for the properties of the condensate directly, or for any changes induced in the condensate by the 2DEG. Going beyond weak coupling theory, the Eliashberg equations [137] must be solved to find the critical temperature, which is not a straightforward task [138].

The aim of this work is not to produce an accurate prediction of the critical temperature in a realistic system, but to demonstrate that the critical temperature may be optically controlled, and that high temperature superconductivity may be possible in these layered systems. The observation of superconductivity in such a system, at any temperature, would be a major discovery, allowing study of this macroscopic coherent phenomena in a precisely controllable setting. The Bose-Fermi system containing a condensate of indirect excitons is likely to simpler to realise experimentally than a microcavity system, and the fixed dipole moment is

also advantageous in leading to enhanced coupling to the 2DEG. Organic-based polariton systems or dipolariton systems may be able to overcome the latter disadvantage however, and would allow study at high temperatures.

My contribution to the work presented in this chapter mainly consisted of extensive work on the calculation of the effective interaction potential and the numerical solution of the gap equation. This work was performed using MATLAB, and in close collaboration with Fabrice Laussy - who worked on the same aspects of the work using Mathematica, in order that we could be confident in the results we obtained independently. I also worked on the extension of the work to the exciton case, and assisted Fabrice Laussy with construction of the analytic, approximate solutions to the gap equation.

Chapter 4

Rotons in a hybrid Bose-Fermi system

The previous chapter demonstrated the great potential of hybrid Bose-Fermi systems for the observation of superconductivity, a macroscopic quantum effect of a fermionic system. In this chapter, the effect of the Bose-Fermi coupling on the bosonic component of the system is studied, and in particular the effects on its coherent superfluid properties. It is shown that coupling between the two subsystems may lead to a significant qualitative change in the excitation spectrum of the condensate, due to modification of the effective interaction [139].

The particular bosonic subsystem considered will be a coupled QW structure in which a condensate of indirect excitons is created. As discussed earlier, in the low density regime, systems of excitons may undergo condensation to a macroscopic coherent state. A condensate of indirect excitons may be described as a weakly interacting Bose gas, with repulsive interactions and hence an excitation dispersion relation which is linear at small momenta, and parabolic at large momenta, as derived by Bogoliubov in the general case [26]. The strong fixed dipole of indirect

excitons allows efficient coupling with a 2DEG - the fermionic component in the hybrid Bose-Fermi system - which may modify the effective interactions within the condensate to such an extent that the dispersion ceases to be Bogoliubov-like. For this reason, the weak coupling theory used in the previous chapter is not suitable, and the effective interaction should be calculated by properly taking into account the effects in both subsystems. The excited states of interest for superconductivity are those states with wavevectors comparable to the Fermi wavevector; at these high wavevectors the excitation dispersion is essentially parabolic, while the effect studied in this chapter is observed at relatively low wavevectors.

In this chapter, a diagrammatic approach is applied in the random-phase approximation (RPA), to find the effective interactions - including higher order processes which create virtual excitations in one or both of the subsystems. This approach accounts for screening effects, in addition to the renormalisation of the excitation spectra and changes in the effective interactions between and within each component.

4.1 Effective interaction

In the random phase approximation, the effective interaction between electrons in an electron gas is given by [78]

$$V_{\text{eff}}(\mathbf{q},\omega) = \frac{V(\mathbf{q})}{1-\Pi(\mathbf{q},\omega)V(\mathbf{q})} = \frac{V(\mathbf{q})}{\epsilon(\mathbf{q},\omega)} \ , \tag{4.1}$$

where $\Pi(\mathbf{q},\omega)$ and $\epsilon(\mathbf{q},\omega)$ are the polarisation function and dielectric function, derived self-consistently in the RPA, and $V(\mathbf{q})$ is simply the bare Coulomb potential in Fourier space. The RPA was introduced for the electron gas by Bohm and Pines [140], and consists of taking all the first order corrections to the Coulomb potential within many-body perturbation theory, as well as the subset of higher order processes which can be obtained as combinations of first order corrections (often called ring diagrams due to their depiction in Feynman diagrams).

This may be generalised to other systems as can be seen by considering a diagrammatic approach, which can be used to justify the RPA more generally [141, 142]. In the system studied here, processes involving both components must be included; for instance excitons may interact directly, or through the creation of virtual excitations in either of the two subsystems (the electronic or excitonic components). Thus the effective interaction between excitons (labelled component 2), may be written

$$V_{22}^{\text{eff}} = V_{22} + \Pi_1 V_{12}^2 + \Pi_2 V_{22}^2 + \Pi_1^2 V_{12}^2 V_{11} + 2\Pi_1\Pi_2 V_{12}^2 V_{22} + \Pi_2^2 V_{22}^3 + \ldots \qquad (4.2)$$

This equation in diagrammatic form is shown in Fig. 4.1. The equations for the effective electron-exciton and electron-electron interactions may be written analo-

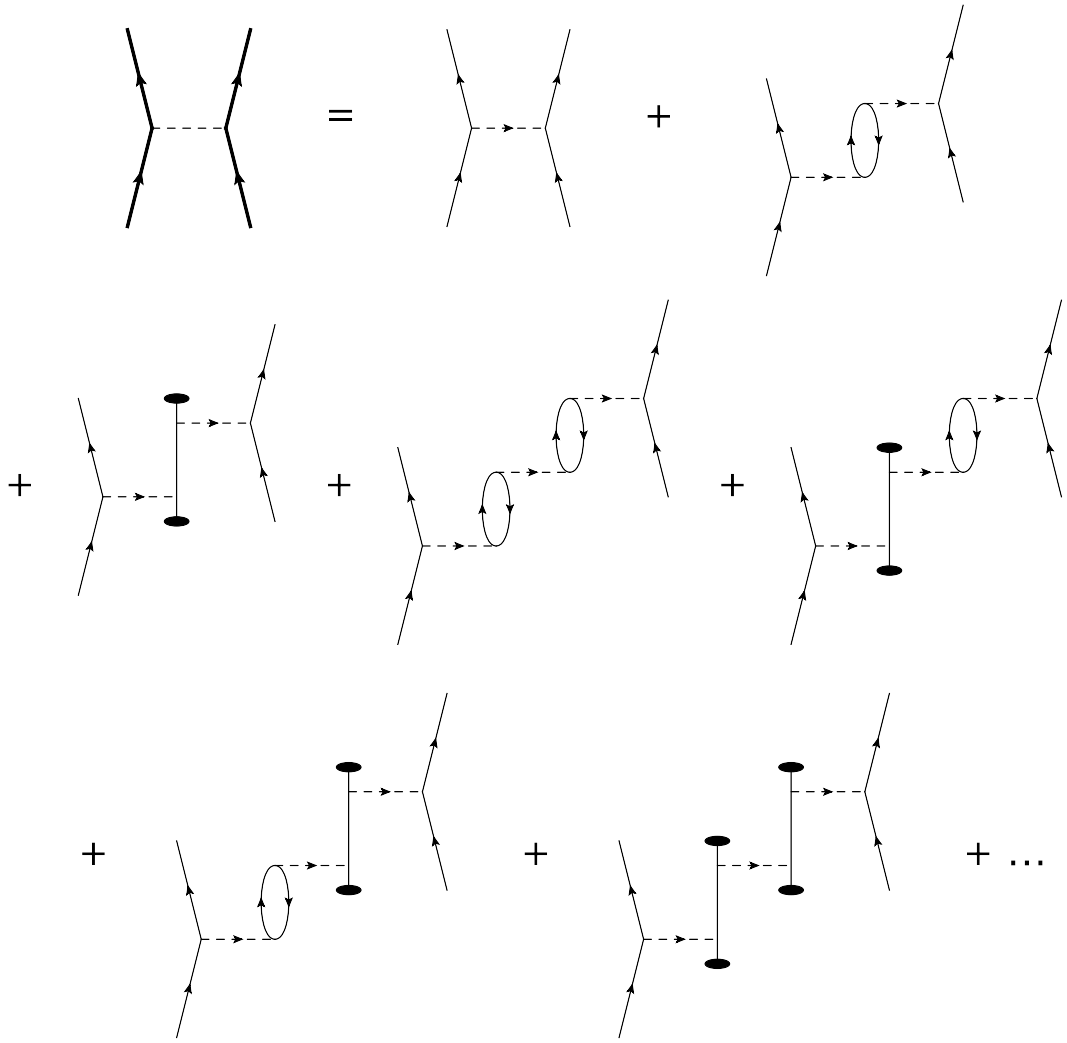

Figure 4.1: The effective exciton-exciton interaction represented diagrammatically in the random-phase approximation. Excitations of the 2DEG are shown as loops, while excitations of the condensate are indicated by black dots.

gously:

$$V_{12}^{\text{eff}} = V_{12} + \Pi_1 V_{11} V_{12} + \Pi_2 V_{12} V_{22} + \Pi_1^2 V_{11}^2 V_{12} + \Pi_2^2 V_{12} V_{22}^2 + \Pi_1 \Pi_2 V_{11} V_{12} V_{22} + \Pi_1 \Pi_2 V_{12}^3 + ..., \tag{4.3}$$

$$V_{11}^{\text{eff}} = V_{11} + \Pi_1 V_{11}^2 + \Pi_2 V_{12}^2 + \Pi_1^2 V_{11}^3 + 2\Pi_1 \Pi_2 V_{11} V_{12}^2 + \Pi_2^2 V_{12}^2 V_{22} + ... \tag{4.4}$$

These three equations may then be combined in matrix form as

$$\mathbf{V}^{\text{eff}} = \mathbf{V} \cdot (\mathbf{I} + \mathbf{\Pi V} + (\mathbf{\Pi V})^2 + \cdots) = \mathbf{V} \cdot (\mathbf{I} - \mathbf{\Pi V})^{-1} , \tag{4.5}$$

where $\mathbf{I}$ is the 2×2 identity matrix. Note the second equality comes from the expression for a convergent geometric series. The matrices $\mathbf{V}, \mathbf{\Pi}$ are given by

$$\mathbf{V} = \begin{pmatrix} V_{11} & V_{12} \\ V_{12} & V_{22} \end{pmatrix} , \tag{4.6}$$

$$\mathbf{\Pi} = \begin{pmatrix} \Pi_1 & 0 \\ 0 & \Pi_2 \end{pmatrix} . \tag{4.7}$$

The bare electron-electron interaction, $V_{\text{C}} = V_{11}$, is described by the standard 2D Coulomb potential, Eq. 1.8, the bare exciton-electron interaction, V_{12}, is given by Eq. 1.14, while the exciton-exciton matrix element, V_{22}, is given by Eq. 1.15. The

polarisation operator for the electron subsystem in the RPA is given by [78]

$$\Pi_1(\mathbf{q},\omega) = \sum_{\mathbf{k}} \frac{f_{\mathbf{k}-\mathbf{q}} - f_{\mathbf{k}}}{\hbar(\omega + i\delta) + E^{\mathrm{el}}_{\mathbf{k}-\mathbf{q}} - E^{\mathrm{el}}_{\mathbf{k}}} \ , \tag{4.8}$$

and for the condensate subsystem [143]

$$\Pi_2(\mathbf{q},\omega) = \frac{2N_0 A E^{\mathrm{ex}}_{\mathbf{q}}}{(\hbar\omega)^2 - (E^{\mathrm{ex}}_{\mathbf{q}})^2} \ , \tag{4.9}$$

where $E^{\mathrm{el}}(q), E^{\mathrm{ex}}(q)$ are the bare electron and exciton dispersion relations, respectively, and $f_{\mathbf{k}}$ is the Fermi-Dirac distribution.

The static approximation is applied for the electron subsystem ($\omega + i\delta \to 0$), which implies [78]

$$\Pi_1(\mathbf{q},\omega) = \frac{A m_{\mathrm{el}}}{\pi\hbar^2}(e^{-\pi\hbar^2 n_{\mathrm{el}}/k_{\mathrm{B}}T m_{\mathrm{el}}} - 1) \ . \tag{4.10}$$

The effective exciton-exciton interaction then reads

$$V^{\mathrm{eff}}_{\mathrm{ex-ex}}(q,\omega) = \frac{\left(V_{22} + \frac{\Pi_1 V_{12}^2(q)}{1-\Pi_1 V_{11}(q)}\right)\left((\hbar\omega)^2 - (E^{\mathrm{ex}}(q))^2\right)}{(\hbar\omega)^2 - (E^{\mathrm{ex}}(q))^2 + 2N_0 A(q) E^{\mathrm{ex}}(q)\left[V_{22} + \frac{\Pi_1 V_{12}^2(q)}{1-\Pi_1 V_{11}(q)}\right]} \ . \tag{4.11}$$

4.2 Excitation spectrum

The poles of this effective potential determine the dispersion of the collective modes of the system, which is therefore given by

$$(\hbar\omega)^2 = (E^{\mathrm{ex}}(q))^2 + 2N_0 A(q) E^{\mathrm{ex}}(q)\left[V_{22} + \frac{\Pi_1 V_{12}^2(q)}{1 - \Pi_1 V_{11}(q)}\right] . \tag{4.12}$$

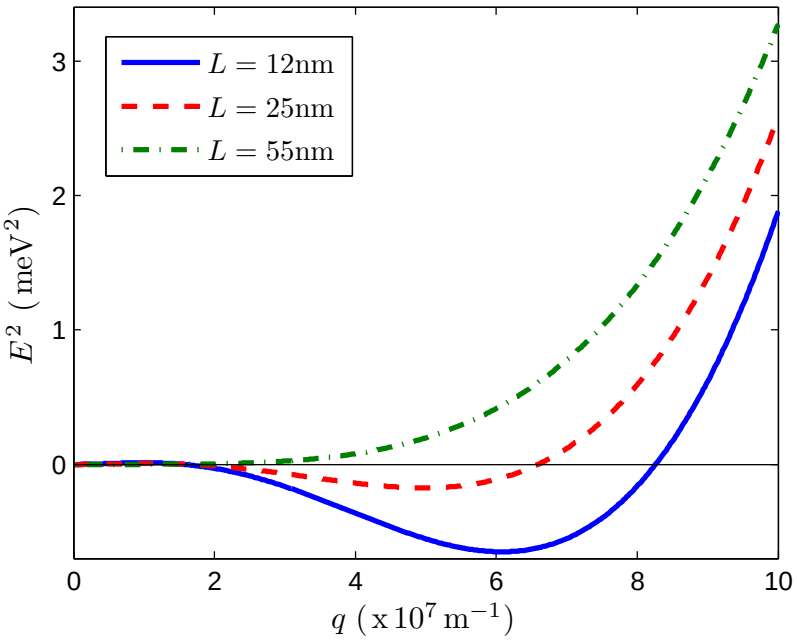

Figure 4.2: Dispersion of the elementary excitations of the condensate, showing a roton minimum. Plotted for parameters of the GaAs-based coupled QW structure studied in [60], assuming that a third n-doped QW is grown at a distance L from the coupled QW structure. The dipole separation $l = 12$nm, $n_s = 1 \times 10^{11}$cm^{-2} and $n_{el} = 4 \times 10^{12}$cm^{-2}.

Figs. 4.2, 4.3 show plots of the dispersion for different values of the condensate density, and separation between the QWs. In some cases the appearance of a roton-like minimum is observed, for some non-zero wavevector. The energy of this roton minimum scales inversely with the exciton concentration, which may of course be optically controlled.

The position and depth of the roton minimum are dependent on the strength of the exciton-exciton interaction, which in turn depends on the separation and on the exciton concentration. At some critical value of the concentration or separation, the energy of the roton minimum is equal to that of the condensate at $q = 0$,

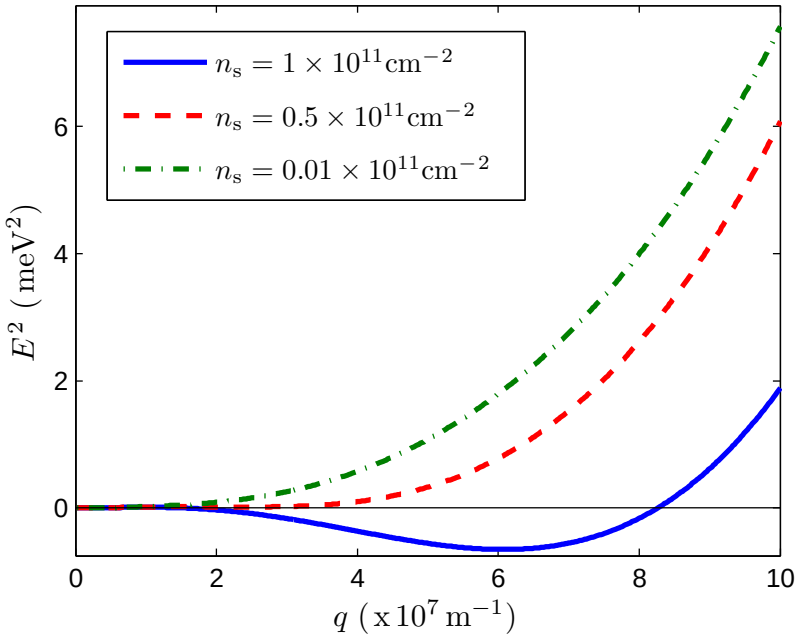

Figure 4.3: Plots of the dispersion illustrating the variation with concentration for $L = 12$nm (other parameters as in previous figure).

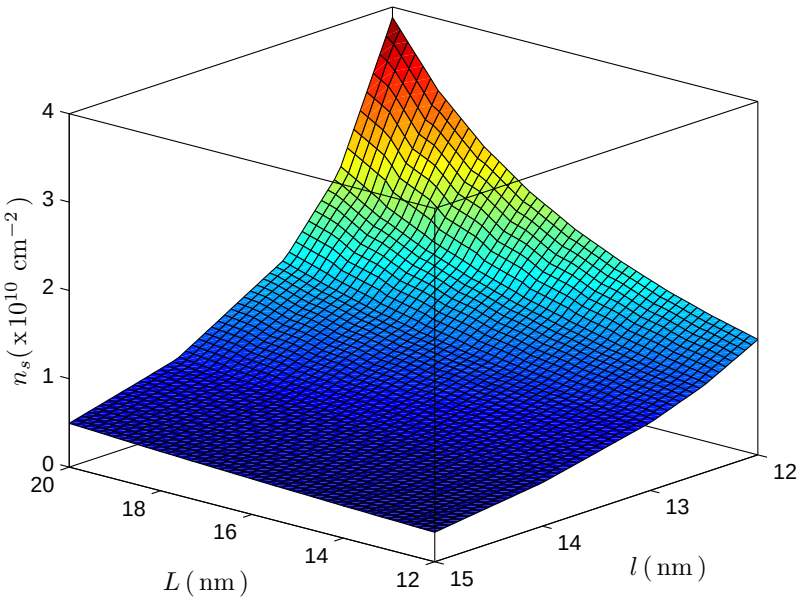

Figure 4.4: Phase diagram of the system - the exciton BEC is unstable above the phase boundary surface and stable below. Plotted for the same structure as the previous figure.

i.e. the roton gap has collapsed. This is manifested as a transition in the system: beyond this point the exciton condensate is unstable and eventually collapses due to escape of excitons towards the roton minimum. The nature of this transition will be investigated in the next chapter.

4.3 Phase transition and finite temperatures

Fig. 4.4 shows the phase diagram for the system, which illustrates that the exciton condensate may collapse at relatively low exciton densities, before the Mott transition is reached.

If the superfluid condensate phase exists at $T = 0$ then it can also be found for finite temperatures up to the Berezinsky-Kosterlitz-Thouless critical temperature, T_{BKT}. At temperatures above T_{BKT}, thermally excited vortices may form in the system and support local order. While below T_{BKT}, bound pairs of vortices exist, which stabilise the phase to a power law decay in distance and support a finite superfluid density, n_{s}. The critical temperature can be found using the formula of Kosterlitz and Nelson [144]:

$$k_{\mathrm{B}} T_{\mathrm{BKT}} = \frac{\pi \hbar^2 n_{\mathrm{s}} \left(T_{\mathrm{BKT}} \right)}{2M}, \tag{4.13}$$

where M is the exciton mass. n_s is given by

$$n_{\mathrm{s}} = n - n_{\mathrm{n}} \left(T_{\mathrm{BKT}} \right), \tag{4.14}$$

where $n = N_0/A$ is the total concentration of excitons, and n_{n} is the normal fraction concentration, which can be estimated as in [42, 145, 146] to be

$$n_{\mathrm{n}} \left(T, n \right) = \frac{\hbar^2}{2\pi M k_{\mathrm{B}} T} \int_0^{\infty} \frac{q^3 e^{\hbar \omega (q) k_{\mathrm{B}} T}}{\left(e^{\hbar \omega (q) k_{\mathrm{B}} T} - 1 \right)^2} dq. \tag{4.15}$$

where $E(q) = \hbar \omega(q)$ is the renormalised dispersion of elementary excitations, given by Eq. 4.12.

The transcendental Eq. 4.13 is solved numerically using MATLAB to carry out the numerical integration and zero finding. Fig. 4.5 shows the dependence of the critical temperature on n and L. For large separations, L, the dependence on concentration is linear, as would be expected for a conventional gas of inter-

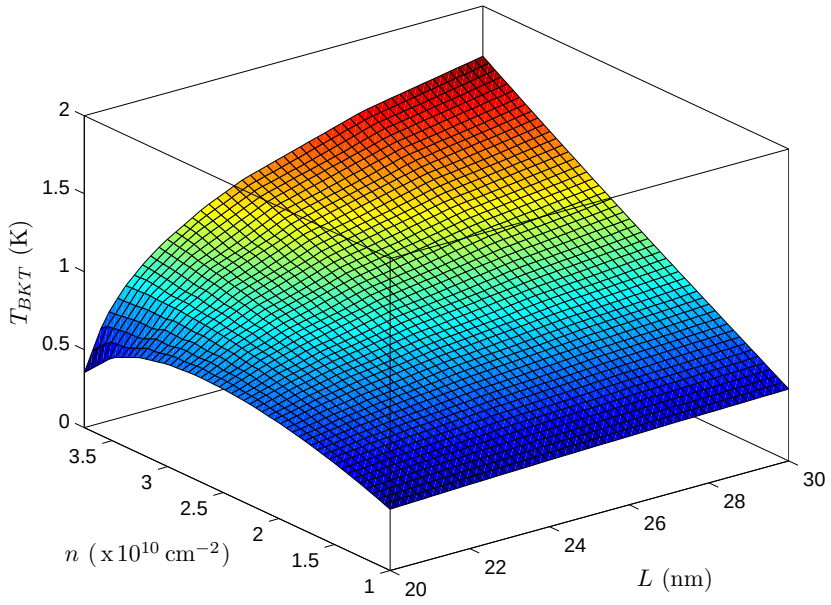

Figure 4.5: Dependence of the BKT critical temperature on concentration and QW separation. Plotted for parameters as in previous figures.

acting bosons. However, for small separation the dependence is non-linear: for small concentrations the critical temperature increases, then decreases at larger concentrations, mirroring the change in strength and sign of the exciton-exciton interaction.

4.4 Summary

In this chapter, the complementary aspect of the Bose-Fermi systems considered in the previous chapter was studied, i.e. the effect of the 2DEG on the bosonic component. However, a different approach was taken in order to calculate the effective interaction within the bosonic component. This was necessary since the inter-component coupling is in this case strong enough to qualitatively alter the spectrum of excitations of the condensate.

A system of indirect excitons has been considered, since their fixed dipole moment allows strong interaction with the 2DEG, compared to the weaker polariton-electron interaction. However, recent works have demonstrated the formation of 'oriented polaritons' [147] and 'dipolaritons' [148] in specially designed microcavity structures, which have greatly enhanced dipole moments, and therefore should interact more efficiently with a 2DEG.

The appearance of a roton minimum in the dispersion of excitations is an interesting fundamental effect, observed in superfluid helium due to strong interactions in the system. It is also interesting due to the possibility that the roton gap may go to zero as the Bose-Fermi coupling is increased; this possibility is studied in the next chapter, examining the state of the bosonic subsystem when the zero

wavevector condensate is no longer the lowest energy state.

My contribution to the work presented in this chapter consisted of checking the diagrammatic derivation of the effective exciton-exciton interaction, which was obtained by Ivan Shelykh; calculating this interaction and the excitation spectrum; and calculating the phase boundary and critical temperatures.

Chapter 5

Exciton supersolidity

In the previous chapter, the possibility of formation of a roton minimum in the spectrum of excitations of an exciton condensate was demonstrated, in a hybrid Bose-Fermi system. If the energy of the roton minimum, at finite wavevector, moves below that of the ground state at zero wavevector, then the ground state of the system ceases to be the zero wavevector condensate, and one would expect the system to undergo a transition to occupy the new ground state. In this chapter, this new ground state is modelled, and shown to exhibit the properties of a *supersolid* phase.

It has previously been suggested that a superfluid to supersolid phase transition may occur due to the appearance of a roton-like instability in a superfluid system [149, 150, 151, 152]. Therefore the hybrid Bose-Fermi system of indirect excitons interacting with a 2DEG seems a promising system for observation of the supersolid phase [153]. In the first section of this chapter, the supersolid phase will be discussed in general, before the specific system is modelled.

5.1 Supersolidity

Originally predicted in 1969 [154, 155], a supersolid is a system in which order in real and reciprocal spaces, in the form of a crystalline lattice, coexists with superfluid behaviour [75, 156]. Over forty years after the theoretical prediction, Kim and Chan published work which claimed to evidence the supersolid phase in ^{4}He by observation of non-classical rotational inertia in torsional oscillator experiments at low temperature [76, 157]. This stimulated other experimental work using different techniques, which complicated the theoretical picture, but which were also presented as providing further evidence for the supersolid phase. Recently, evidence has been presented for a transition to the supersolid phase in cold atom systems [158], due to the closing of a roton gap in the superfluid phase [159].

There has been much debate as to whether the experimental findings of the last decade constitute a 'discovery' of supersolidity (in recent work [160], Davis and coworkers claim to have ruled out the possibility of a supersolid phase transition in ^{4}He), however in principle the supersolid phase may be present in any system of interacting bosons, such as an exciton condensate. Indeed a recent theoretical paper by Parish *et al.* [161] studies the possibility of supersolidity in an excitonic system of asymmetrically populated bilayers.

To recall, the system studied is composed a layer of indirect excitons situated close to a layer containing a 2DEG. This may be realised in a structure of three parallel quantum wells (QWs), one containing a 2DEG, and the other two containing a BEC of spatially indirect excitons, or a metal layer may be deposited in place of the third QW containing the 2DEG. The two subsystems are spatially separated

but close enough to allow efficient Coulomb interaction. The spatial separation presents an advantage over the system considered by Parish *et al.* in that higher densities are possible due to protection from the phase space filling effect. The spin of the exciton is accounted for here, by differentiating between the exciton states which are coupled to light, with spin projections of $+1$ and -1 on the structure growth axis.

5.2 Condensate description

An exciton condensate may be described by a factorised Hartree-Fock ansatz [20]:

$$\Psi_{\pm}(\mathbf{r}_1, \ldots, \mathbf{r}_N, t) = \prod_i \psi_{\pm}(\mathbf{r}_i, t) \ , \tag{5.1}$$

which, in the limit of large number of particles N, leads to the following mean field energy with a nonlocal interaction potential:

$$\begin{aligned} H_{\pm} = N_{\pm} \int d\mathbf{r}\, \psi^*_{\pm}(\mathbf{r}, t) \Bigg(-\frac{\hbar^2}{2m_{\mathrm{ex}}} \nabla^2 \\ + \frac{1}{2} \int d\mathbf{r}' \left(V^{\mathrm{eff}}_{\mathrm{ex-ex}}(\mathbf{r} - \mathbf{r}') n_{\mathrm{tot}}(\mathbf{r}', t) + \alpha n_{\mp}(\mathbf{r}', t) \right) \Bigg) \psi_{\pm}(\mathbf{r}, t) \ . \end{aligned} \tag{5.2}$$

$n_{\mathrm{tot}}(\mathbf{r}, t) = n_+(\mathbf{r}, t) + n_-(\mathbf{r}, t) = N_+ |\psi_+(\mathbf{r}, t)|^2 + N_- |\psi_-(\mathbf{r}, t)|^2$, and $V^{\mathrm{eff}}_{\mathrm{ex-ex}}(\mathbf{r})$ is the spin-isotropic exciton-exciton interaction potential. The exchange interaction is modelled phenomenologically by introducing the constant α. The corresponding

time-dependent Gross-Pitaevskii (GP) equations read

$$i\hbar\frac{\partial\psi_{\pm}(\mathbf{r},t)}{\partial t} = -\frac{\hbar^2\nabla^2}{2m_{\rm ex}}\psi_{\pm}(\mathbf{r},t) \tag{5.3}$$
$$+\int V^{\rm eff}_{\rm ex-ex}(\mathbf{r}-\mathbf{r}')n_{\rm tot}(\mathbf{r}',t)d\mathbf{r}'\psi_{\pm}(\mathbf{r},t) + \alpha n_{\mp}(\mathbf{r},t)\psi_{\pm}(\mathbf{r},t)\ .$$

The expression for the effective exciton-exciton was derived in the previous chapter, and is given by Eq. 4.11. The expression previously taken for the bare exciton-exciton interaction matrix element, V_{22}, is that generally used when modelling polariton and exciton condensates. However, in coupled QW structures, the interaction is modified due to the fixed relative orientation of dipole excitons - leading to a different form for the interaction [162, 163]:

$$V_{22}(q) = \frac{e^2 l\xi}{\epsilon_0\epsilon_{\rm r}A}\ , \tag{5.4}$$

where l is the exciton dipole separation in the normal to the QW plane direction, and ξ accounts for the reduction of dipole-dipole repulsion due to electron-hole pair correlations in the exciton condensate [164].

The effective exciton-exciton interaction is in general a time dependent, retarded interaction, however in order to obtain a non-retarded GP equation (5.3), this dependence is removed by averaging the potential over a frequency range $[0,\omega_{\rm d}]$, where $\omega_{\rm d} = E_{\rm b}/\hbar$ is the exciton dissociation frequency. The resulting potential is plotted in Fig. 5.1 for different values of the separation between the electron and exciton subsystems, L. The corresponding condensate excitation spectrums, given by Eq. 4.12, are plotted in the top part of Fig. 5.1. It can be seen that

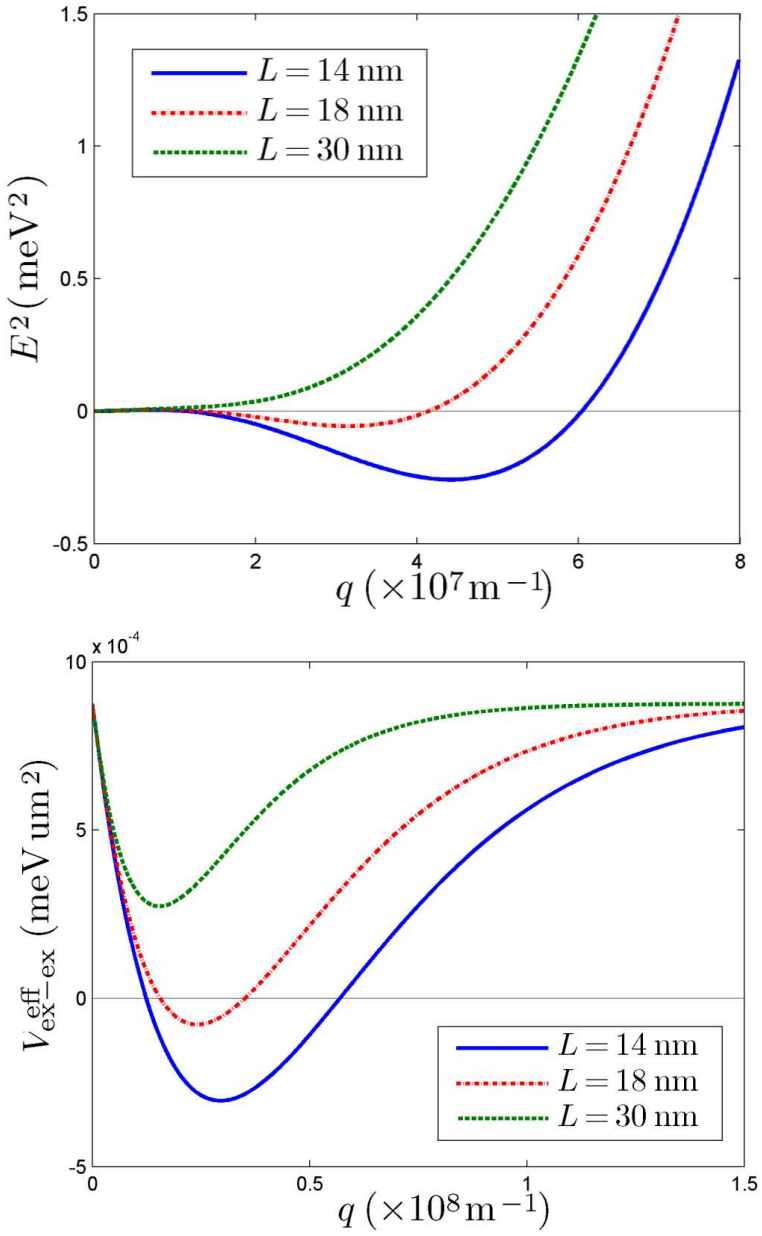

Figure 5.1: The excitation spectrum (top) and effective exciton-exciton interaction potential (bottom) for three values of the exciton-electron layer separation L. The exciton mass, $m_{\mathrm{ex}} = 0.21 m_{\mathrm{e}}$, and the average exciton density $\overline{n}_{\mathrm{ex}} = 1 \times 10^{11}\,\mathrm{cm}^{-2}$.

for small separations the potential becomes attractive in some range of $q > 0$, and a roton instability develops in the excitation spectrum. The presence of the 2DEG alters the dispersion of excitations due to a change in the character of the effective exciton-exciton interaction, which by the creation of virtual excitations in the 2DEG, may become attractive for some q. It is known that condensation is in general unstable to attractive interactions, and therefore the onset of this attraction may simply cause collapse in real space, however it will be shown that for a range of parameters the supersolid phase is the ground state of the system.

5.3 The supersolid phase

As mentioned, the existence of a roton instability has been connected with the possible existence of a supersolid phase. This possibility is investigated by numerical minimisation of the Hamiltonian (5.2), using the imaginary time propagation method to determine the ground state for a two dimensional box, with periodic boundary conditions and realistic parameters. As a first step, the exciton spin is neglected, assuming $\alpha = 0$ and considering a single component condensate.

In Fig. 5.2 the results of the minimisation are illustrated as density profiles of the exciton condensate in real and reciprocal space. For large separations, the excitation spectrum does not cross below the zero energy axis, i.e. there is no roton minimum or there is a positive roton gap. In this case the ground state is a homogeneous superfluid, as shown in Figs. 5.2(a) and (b) for $L = 30\,\mathrm{nm}$. As the separation is decreased, the roton gap is reduced until a critical separation where the roton gap disappears. For a separation of $L = 18\,\mathrm{nm}$, the ground

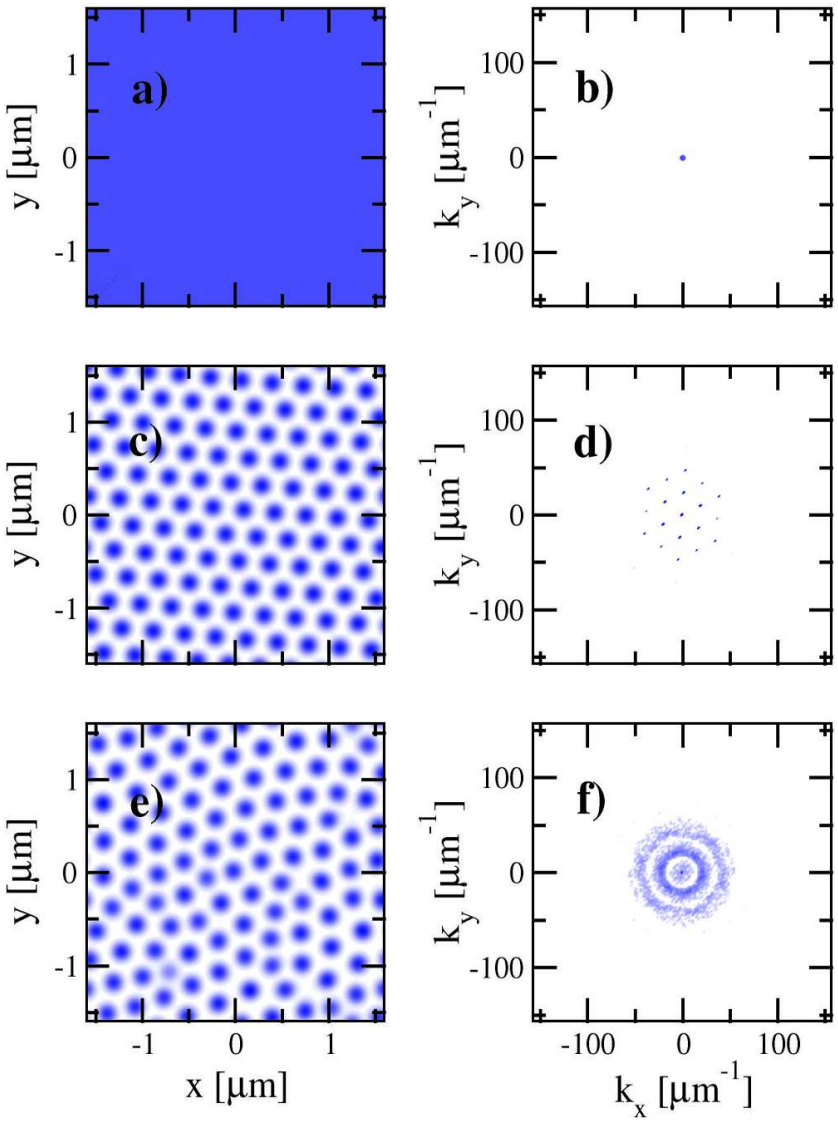

Figure 5.2: Examples of density profiles of the exciton condensate in real space (left column) and reciprocal space (right column, density in logarithmic scale). The figures (a), (b) show the homogeneous ground state for separation $L = 30\,\mathrm{nm}$, and the figures (c), (d) depict the supersolid ground state for $L = 18\,\mathrm{nm}$, characterised by periodicity in both real and momentum spaces. The orientation of the supersolid lattice is chosen spontaneously. (e), (f) A metastable state with lattice imperfections, corresponding to a local energy minimum. In momentum space, such a state is characterized by concentric rings.

state is completely changed, as shown in Figs. 5.2(c) and (d). In real space the ground state is characterised by a triangular lattice, where the orientation is chosen randomly in a spontaneous symmetry breaking process. Note that this symmetry breaking is additional to that which occurs in determination of the condensate wavefunction. In reciprocal space, side peaks are observed corresponding to the lattice wavevectors. The lattice constant of the pattern is determined by the value of the wavevector at the roton minimum. Decreasing the separation further to $L = 14\,\mathrm{nm}$, the minimisation procedure leads to collapse of the wavefunction into a single point of the numerical grid, indicating breakdown of the model. In order to obtain the correct ground state of the system, one would need to include higher order effects which would prevent the condensate density from growing without bound. It is not surprising that collapse is encountered, since this is generally the case for a nonlinear Schrödinger equation with attractive nonlinearity [165].

Figs. 5.2(e) and (f) show another type of solution produced by the minimisation procedure, for $L = 18\,\mathrm{nm}$, but with different initial noise to that which leads to the solutions shown in Figs. 5.2(c) and (d). These solutions are characterised by a crystal structure with dislocations, and are not true ground states, but metastable states at local minima of the energy. They are interesting from an experimental point of view, since they would be likely to be observed, perhaps even more so due to the disorder potential present in real samples. In reciprocal space, these distorted supersolid states are characterised by concentric rings around zero wavevector, as shown in Fig. 5.2(f).

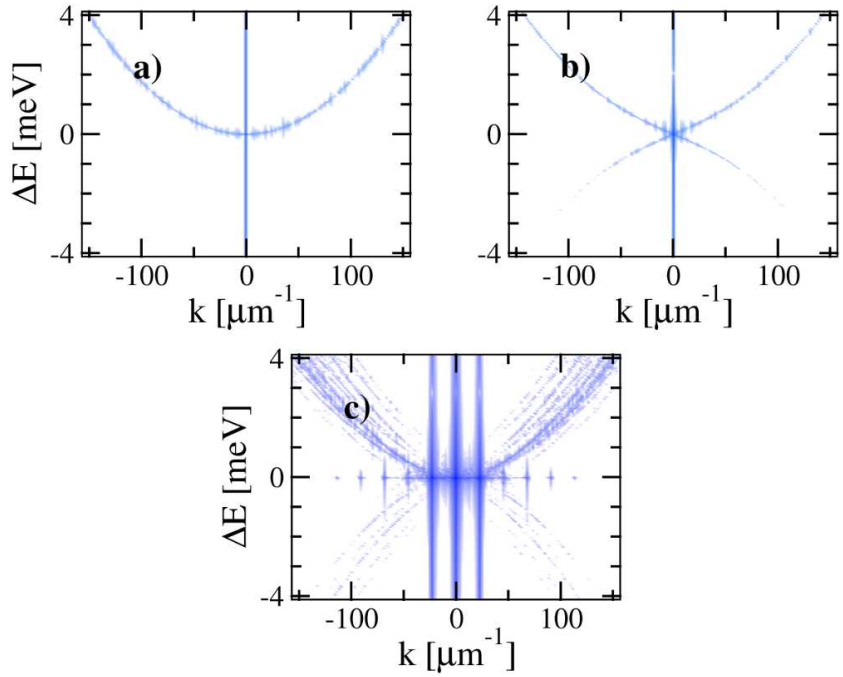

Figure 5.3: Numerically determined spectra of a weakly perturbed condensate in three different regimes: (a) noninteracting exciton condensate, (b) condensate interacting through a local (momentum independent) potential, and (c) supersolid condensate in the presence of coupling with an electron gas, interacting through an effective potential $V^{\mathrm{eff}}_{\mathrm{ex-ex}}$ (with parameters as in Figs. 5.2(c),(d)). In cases (a) and (b) the parabolic and Bogoliubov spectra are obtained as predicted theoretically. In case (c) the spectrum is distorted as a result of interference of branches starting from different k-components of the ground state in the momentum space, corresponding to the vertical lines. The density is shown in a logarithmic intensity scale.

5.4 Excited states

It is also interesting to investigate the influence of the supersolid transition on a weakly excited system. Fig. 5.3 shows the spectra of perturbed ground states allowed to evolve in time according to Eq. (5.3). The spectra is obtained by Fourier transformation of the wavefunction ψ in space and time. Fig. 5.3(a) shows the

spectrum for a noninteracting exciton condensate, which is parabolic as expected. In Fig. 5.3(b) a q-independent interaction potential is present, equivalent to a repulsive contact interaction in the absence of a 2DEG. The spectrum is the expected Bogoliubov spectrum of excitations, linear for small wavevectors, and parabolic at larger wavevectors. Fig. 5.3(c) corresponds to the more interesting case of the full wavevector dependent interaction $V^{\text{eff}}_{\text{ex}-\text{ex}}$, in the supersolid regime. The spectra here is blurred, due to interference of multiple branches starting from different points in the momentum space. These correspond to the momentum space components of the ground state, which are visible as vertical lines. Despite this blurring, the excitation branches do appear linear close to their origins, indicating a finite superfluid fraction.

The two component case is now returned to, with finite exchange interaction α. Fig. 5.4 shows the real space distribution of excitons in the parameter range leading to the supersolid phase. The two spin components are coloured differently, showing the domains of spin polarisation formed, analogous to ferromagnetic domains. The boundaries between these domains are stochastic and change depending on the initial numerical noise.

5.5 Summary

In this chapter, the existence of an exotic quantum phase transition in a hybrid Bose-Fermi system has been studied. The system considered is composed of indirect excitons interacting with an electron gas. Indirect excitons have been considered due to their large fixed dipole moment, which allows efficient interaction

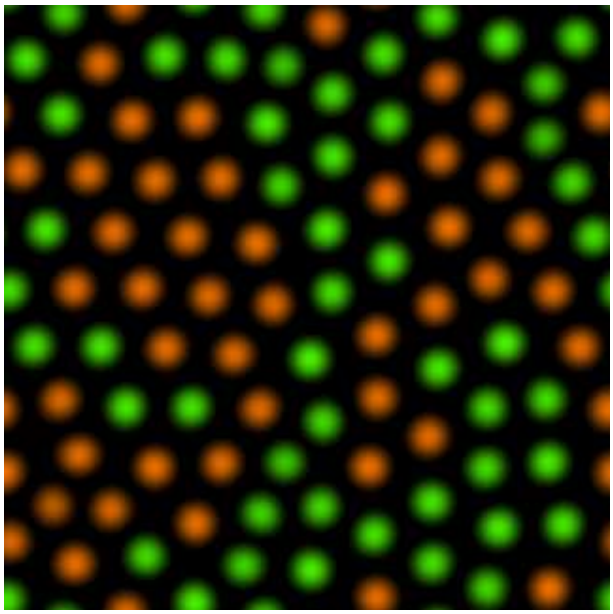

Figure 5.4: Calculated density distribution of the excitonic condensate in the supersolid regime, demonstrating a ferromagnetic domain structure. The interaction constant α is chosen in such a way that for $q = 0$ the interaction of excitons with opposite spin is 10% stronger than the interaction of excitons with parallel spins. The $+1$ and -1 spin components are shown in green and orange, respectively.

with electrons, such that the effective interaction within the exciton condensate is fundamentally altered, acquiring an attractive nature in contrast to the repulsive dipole interaction in an isolated exciton condensate. The prediction of this supersolid phase of excitons may be comparatively easy to observe, when compared to the complications in the interpretation of experiments with superfluid helium.

The new ground state was studied by numerical solution of the Gross-Pitaevskii equation for the condensate wavefunction, accounting for the spin degree of freedom phenomenologically. Experimental detection of an exciton supersolid may be achieved by angularly resolved photoluminescence, which would give access to the characteristic diffraction pattern in the Fourier spectrum of excitations, shown in Fig. 5.3, (d) and (f).

My contribution to the work presented in this chapter consisted mainly of generation of the effective exciton-exciton interaction potential for the various cases of interest.

Chapter 6

Conclusion

This thesis has examined a series of quantum coherent effects in microcavity and indirect exciton systems. The study of condensation in these systems is an extremely interesting subject in its own right, due to the peculiar nature of excitonic systems compared to other condensed matter systems: excitonic systems demonstrate many unique complexities compared to the picture of Bose-Einstein condensation of cold atoms, but are also highly accessible and controllable systems, due to the coupling to the light field.

This makes these systems particularly useful for exploitation of condensation and quantum coherent effects in applications, up to and above room temperature. The polariton laser has great potential as an application of microcavity systems, due to the ultralow threshold this laser may achieve, while there are also many applications which may arise from the manipulation of polariton condensates in information processing - using optical integrated circuits where information is encoded in the polariton spin, and the nonlinearity of polaritons is exploited in elements such as switches and transistors.

Chapter two of this thesis considered a useful potential application of condensa-

tion in microcavity polariton systems, where a polariton condensate stimulates a terahertz transition in order to overcome the general obstacle of slow spontaneous emission in terahertz transitions. The terahertz transition is given by the decay of a $2p$ exciton to a condensate at the bottom of the lower polariton branch; the $2p$ exciton must be excited using two-photon pumping in order to conserve orbital angular momentum, and for a threshold population terahertz lasing may occur simultaneously with polariton lasing. The study of this application also led to the prediction of an associated fundamental effect: the dependence of the threshold to the statistics of the pump.

The rest of the thesis considered the interaction of an excitonic condensate with a gas of carriers in hybrid Bose-Fermi systems. These systems have only recently begun to be studied, but allow the consideration of a number of different bosonic and fermionic effects within a single system, while enabling the exploitation of Bose-Fermi coupling in order to tune the interactions and parameters within each component. A hybrid Bose-Fermi system may be considered from two complementary viewpoints; firstly studying the effect of interaction with a condensate on a fermionic component of electrons - and in particular the influence on the transport properties of this subsystem. Controllable modification of the transport properties may be useful as a way of harnessing the coherent properties of excitonic condensates in information processing, using the charge degree of freedom rather than spin.

Chapter three examines Bose-Fermi systems from this point of view and shows that in fact interaction with an excitonic condensate may induce a pairing interaction in a 2DEG, leading to superconductivity. The electronic component is modelled

using BCS theory, and an effective electron-electron interaction derived which may be attractive and which scales with the condensate density, allowing optical control of the critical temperature for superconductivity.

The remaining two chapters then studied the complementary perspective, that is the effect of interaction with a 2DEG on an excitonic condensate. The effective interactions within the system were modelled fully in the random phase approximation, and it was shown that the exciton-exciton interaction may become attractive due to higher order scattering processes involving virtual excitations of the 2DEG. This results in the appearance of a roton minimum in the dispersion of excitations of the condensate, with a gap to the ground state energy which is dependent on the condensate density and separation between the condensate and 2DEG. A natural question is then what occurs when the roton gap disappears; this question was examined using the Gross-Pitaevskii equation to obtain the new condensate ground state, which was shown to be a supersolid phase.

The thesis as a whole has demonstrated the potential of hybrid Bose-Fermi systems for the study of macroscopic quantum effects; these systems have hardly been studied and the experimental realisation of such a system would be extremely interesting, and would likely lead to the observation of effects which have not yet been considered theoretically.

The main original results of this thesis can be summarised as follows:

- the proposal of terahertz lasing from a microcavity system, demonstrating significant advantages over existing terahertz lasers;
- the demonstration of the potential of hybrid Bose-Fermi systems for obser-

vation of unconventional superconductivity;

- the prediction of a qualitative change to the dispersion of elementary excitations in a superfluid exciton condensate interacting with a 2DEG;
- the prediction of a transition to the exciton supersolid phase in this system.

Appendix A

Parameters used in Chapter 3

Parameter	Meaning	Value
ϵ_{r}	Relative permittivity	7
β_e	Electron reduced mass	$\frac{0.22}{0.22+1.25} \approx 1.15$
β_h	Hole reduced mass	$\frac{1.25}{0.22+1.25} \approx 0.85$
L	Distance between wells	5 nm
κ	Screening wavenumber	$\approx 1.2 \times 10^9$ m^{-1}
m_{x}	Exciton mass	$(0.22 + 1.25)m_0$
m_{c}	Photon mass	$10^{-5}m_0$
X	Hopfield coefficient (exciton weight)	$1/\sqrt{2}$ [1]
$2g$	Rabi splitting	45 meV [0]
k_{F}	Fermi wavevector	5×10^8 m^{-1}
a_{B}	Exciton Bohr radius	1.98×10^{-9} m
E_{b}	Exciton binding energy	32 meV
l	Dipole separation	4 nm [12]

Table A.1: Parameters used in numerical calculations, where m_0 is the vacuum electron mass. In square brackets, the value for the exciton case when the parameter differs from the polariton case, otherwise parameters have been taken the same for comparison.

Bibliography

[1] J. Frenkel. On the Transformation of light into Heat in Solids. I. *Physical Review*, 37(1):17–44, 1931.

[2] G. H. Wannier. The Structure of Electronic Excitation Levels in Insulating Crystals. *Physical Review*, 52(3):191–197, 1937.

[3] N. F. Mott. Conduction in polar crystals. II. The conduction band and ultra-violet absorption of alkali-halide crystals. *Transactions of the Faraday Society*, 34:500–506, 1938.

[4] A. V. Kavokin, J. J. Baumberg, G. Malpuech, and F. P. Laussy. *Microcavities*. Oxford University Press, New York, 2007.

[5] C. Weisbuch, M. Nishioka, A. Ishikawa, and Y. Arakawa. Observation of the coupled exciton-photon mode splitting in a semiconductor quantum microcavity. *Physical Review Letters*, 69(23):3314–3317, 1992.

[6] A. V. Kavokin. Exciton-polaritons in microcavities: present and future. *Applied Physics A*, 89(2):241–246, 2007.

[7] Jeremy J Baumberg, Pavlos G Savvidis, Pavlos.G Lagoudakis, M.D Martin, David Whittaker, R Butte, Maurice Skolnick, and John Roberts. Polariton

traps in semiconductor microcavities. *Physica E: Low-dimensional Systems and Nanostructures*, 13(2-4):385–389, 2002.

[8] A. V. Kavokin and B. Gil. GaN microcavities: Giant Rabi splitting and optical anisotropy. *Applied Physics Letters*, 72(22):2880, 1998.

[9] L. Kappei, J. Szczytko, F. Morier-Genoud, and B. Deveaud. Direct Observation of the Mott Transition in an Optically Excited Semiconductor Quantum Well. *Physical Review Letters*, 94(14):147403, 2005.

[10] N. F. Mott. The Basis of the Electron Theory of Metals, with Special Reference to the Transition Metals. *Proceedings of the Physical Society. Section A*, 62(7):416–422, 1949.

[11] Le Si Dang, D. Heger, R. André, F. Boeuf, and R. Romestain. Stimulation of Polariton Photoluminescence in Semiconductor Microcavity. *Physical Review Letters*, 81(18):3920–3923, 1998.

[12] P. G. Savvidis, J. J. Baumberg, R. M. Stevenson, M. S. Skolnick, D. M. Whittaker, and J. S. Roberts. Angle-Resonant Stimulated Polariton Amplifier. *Physical review letters*, 84(7):1547–1550, 2000.

[13] J. J Baumberg, P. G. Savvidis, R. M Stevenson, A. I Tartakovskii, M. S Skolnick, D. M Whittaker, and J. S Roberts. Parametric oscillation in a vertical microcavity: A polariton condensate or micro-optical parametric oscillation. *Physical Review B*, 62(24):R16247–R16250, 2000.

[14] H. Deng, H. Haug, and Y. Yamamoto. Exciton-polariton Bose-Einstein condensation. *Reviews of Modern Physics*, 82(2):1489–1537, 2010.

[15] J. Keeling, F. M. Marchetti, M. H. Szymaska, and P. B. Littlewood. Collective coherence in planar semiconductor microcavities. *Semiconductor Science and Technology*, 22(5):R1–R26, 2007.

[16] A. Das, J. Heo, M. Jankowski, W. Guo, L. Zhang, H. Deng, and P. Bhattacharya. Room Temperature Ultralow Threshold GaN Nanowire Polariton Laser. *Physical Review Letters*, 107(6):066405, 2011.

[17] T. C. H. Liew, A. V. Kavokin, and I. Shelykh. Optical Circuits Based on Polariton Neurons in Semiconductor Microcavities. *Physical Review Letters*, 101(1):016402, 2008.

[18] T. C. H. Liew, A. V. Kavokin, M. A. Kaliteevski, I. A. Shelykh, R. A. Abram, and T. Ostatnický. Exciton-polariton integrated circuits. *Physical Review B*, 82(3):033302, 2010.

[19] A. V. Kavokin. Exciton-polaritons in microcavities: Recent discoveries and perspectives. *Physica Status Solidi (B)*, 247(8):1898–1906, 2010.

[20] A. J. Leggett. Bose-Einstein condensation in the alkali gases: Some fundamental concepts. *Reviews of Modern Physics*, 73(2):307–356, 2001.

[21] X. Zhu, P. B. Littlewood, M. S. Hybertsen, and T. M. Rice. Exciton Condensate in Semiconductor Quantum Well Structures. *Physical Review Letters*, 74(9):1633–1636, 1995.

[22] A. L. Ivanov. Quantum diffusion of dipole-oriented indirect excitons in coupled quantum wells. *Europhysics Letters*, 59(4):586–591, 2002.

[23] L. V. Butov. Cold exciton gases in coupled quantum well structures. *Journal of Physics: Condensed Matter*, 19(29):295202, 2007.

[24] L. V. Butov and A. V. Kavokin. The behaviour of exciton-polaritons. *Nature Photonics*, 6(1):2, 2012.

[25] B. Deveaud-Plédran. On the condensation of polaritons. *Journal of the Optical Society of America B*, 29(2):A138–A145, 2012.

[26] N. N. Bogoliubov. On the Theory of Superfluidity. *Journal of Physics (USSR)*, 11(1):23–32, 1947.

[27] O. Penrose and L. Onsager. Bose-Einstein Condensation and Liquid Helium. *Physical Review*, 104(3):576–584, 1956.

[28] C. N. Yang. Concept of Off-Diagonal Long-Range Order and the Quantum Phases of Liquid He and of Superconductors. *Reviews of Modern Physics*, 34(4):694–704, 1962.

[29] M H Anderson, J R Ensher, M R Matthews, C E Wieman, and E a Cornell. Observation of bose-einstein condensation in a dilute atomic vapor. *Science (New York, N.Y.)*, 269(5221):198–201, July 1995.

[30] K. B. Davis, M.-O. Mewes, M. R. Andrews, N. J. van Druten, D. S. Durfee, D. M. Kurn, and W. Ketterle. Bose-Einstein Condensation in a Gas of Sodium Atoms. *Physical Review Letters*, 75(22):3969–3973, 1995.

[31] P. Kapitza. Viscosity of Liquid Helium below the λ-Point. *Nature*, 141(3558):74, 1938.

[32] J. F. Allen and A. D. Misener. Flow of Liquid Helium II. *Nature*, 141(3558):75, 1938.

[33] F. London. The λ-Phenomenon of Liquid Helium and the Bose-Einstein Degeneracy. *Nature*, 141(3571):643–644, 1938.

[34] G. B. Hess and W. M. Fairbank. Measurements of Angular Momentum in Superfluid Helium. *Physical Review Letters*, 19(5):216–218, 1967.

[35] A. J. Leggett. Superfluidity. *Reviews of Modern Physics*, 71(2):S318–S323, 1999.

[36] L. D. Landau. The Theory of Superfluid Helium II. *Journal of Physics (USSR)*, 5:71, 1941.

[37] R. P. Feynman. Atomic Theory of the Two-Fluid Model of Liquid Helium. *Physical Review*, 94(2):262–277, 1954.

[38] J. L. Yarnell, G. P. Arnold, P. J. Bendt, and E. C. Kerr. Energy vs Momentum Relation for the Excitations in Liquid Helium. *Physical Review Letters*, 1(1):9–11, 1958.

[39] R. J. Donnelly, J. A. Donnelly, and R. N. Hills. Specific heat and dispersion curve for helium II. *Journal of Low Temperature Physics*, 44(5-6):471–489, 1981.

[40] N. D. Mermin and H. Wagner. Absence of Ferromagnetism or Antiferromagnetism in One- or Two-Dimensional Isotropic Heisenberg Models. *Physical Review Letters*, 17(22):1133–1136, 1966.

[41] P. C. Hohenberg. Existence of Long-Range Order in One and Two Dimensions. *Physical Review*, 158(2):383–386, 1967.

[42] A. Posazhennikova. Colloquium: Weakly interacting, dilute Bose gases in 2D. *Reviews of Modern Physics*, 78(4):1111–1134, 2006.

[43] V. L. Berezinskii. Destruction of long-range order in one-dimensional and two-dimensional systems possessing a continuous symmetry group. II. Quantum systems. *Soviet Physics JETP*, 34:610–616, 1972.

[44] J. M. Kosterlitz and D. J. Thouless. Ordering , metastability and phase transitions in two-dimensional systems. *J. Phys. C: Solid State Phys.*, 6:1181, 1973.

[45] T. P. Simula and P. B. Blakie. Thermal Activation of Vortex-Antivortex Pairs in Quasi-Two-Dimensional Bose-Einstein Condensates. *Physical Review Letters*, 96(2):020404, 2006.

[46] G. Malpuech, Y. G. Rubo, F. P. Laussy, P Bigenwald, and A. V. Kavokin. Polariton laser: thermodynamics and quantum kinetic theory. *Semiconductor Science and Technology*, 18(10):S395–S404, 2003.

[47] A. Imamoğlu and R. J. Ram. Quantum dynamics of exciton lasers. *Physics Letters A*, 214(3-4):193–198, 1996.

[48] P. Senellart and J. Bloch. Nonlinear Emission of Microcavity Polaritons in the Low Density Regime. *Physical Review Letters*, 82(6):1233–1236, 1999.

[49] S. Christopoulos, G. Baldassarri Höger von Högersthal, A. J. D. Grundy, P. G. Lagoudakis, A. V. Kavokin, J. Baumberg, G. Christmann, R. Butté,

E. Feltin, J.-F. Carlin, and N. Grandjean. Room-Temperature Polariton Lasing in Semiconductor Microcavities. *Physical Review Letters*, 98(12):126405, 2007.

[50] J. Levrat, R. Butté, E. Feltin, J.-F. Carlin, N. Grandjean, D. D. Solnyshkov, and G. Malpuech. Condensation phase diagram of cavity polaritons in GaN-based microcavities: Experiment and theory. *Physical Review B*, 81(12):125305, 2010.

[51] E. Wertz, L. Ferrier, D. D. Solnyshkov, R. Johne, D. Sanvitto, A. Lemaître, I. Sagnes, R. Grousson, A. V. Kavokin, P. Senellart, G. Malpuech, and J. Bloch. Spontaneous formation and optical manipulation of extended polariton condensates. *Nature Physics*, 6(11):860–864, 2010.

[52] J. Kasprzak, M. Richard, S. Kundermann, A. Baas, P. Jeambrun, J. Keeling, F. M. Marchetti, M. H. Szymaska, R. André, J. L. Staehli, V. Savona, P. B. Littlewood, B. Deveaud, and Le Si Dang. Bose-Einstein condensation of exciton polaritons. *Nature*, 443(7110):409–414, 2006.

[53] R. Balili, V. Hartwell, D. Snoke, L. Pfeiffer, and K. West. Bose-Einstein condensation of microcavity polaritons in a trap. *Science*, 316(5827):1007–1010, 2007.

[54] J. J. Baumberg, A. V. Kavokin, S. Christopoulos, A. J. D. Grundy, R. Butté, G. Christmann, D. D. Solnyshkov, G. Malpuech, G. Baldassarri Höger von Högersthal, E. Feltin, J.-F. Carlin, and N. Grandjean. Spontaneous Polarization Buildup in a Room-Temperature Polariton Laser. *Physical Review Letters*, 101(13):136409, 2008.

[55] G. Christmann, R. Butte, E. Feltin, J.-F. Carlin, and N. Grandjean. Room temperature polariton lasing in a GaN/AlGaN multiple quantum well microcavity. *Applied Physics Letters*, 93(5):051102, 2008.

[56] J. Kasprzak, D. D. Solnyshkov, R. André, Le Si Dang, and G. Malpuech. Formation of an Exciton Polariton Condensate: Thermodynamic versus Kinetic Regimes. *Physical Review Letters*, 101(14):146404, 2008.

[57] D. Read, T. C. H. Liew, Y. G. Rubo, and A. V. Kavokin. Stochastic polarization formation in exciton-polariton Bose-Einstein condensates. *Physical Review B*, 80(19):195309, 2009.

[58] H. Ohadi, E. Kammann, K. G. Lagoudakis, A. V. Kavokin, and P. G. Lagoudakis. Spontaneous symmetry breaking in a polariton and photon laser. *arXiv*, 1204.5969, 2012.

[59] M. O. Borgh, J. Keeling, and N. G. Berloff. Spatial pattern formation and polarization dynamics of a nonequilibrium spinor polariton condensate. *Physical Review B*, 81(23):235302, 2010.

[60] L. V. Butov, A. C. Gossard, and D. S. Chemla. Macroscopically ordered state in an exciton system. *Nature*, 418(6899):751–754, 2002.

[61] L. V. Butov. Exciton condensation in coupled quantum wells. *Solid State Communications*, 127(2):89–98, 2003.

[62] D. W. Snoke. Coherence and Optical Emission from Bilayer Exciton Condensates. *Advances in Condensed Matter Physics*, 2011:938609, 2011.

[63] A. A. High, J. R. Leonard, A. T. Hammack, M. M. Fogler, L. V. Butov,

A. V. Kavokin, K. L. Campman, and A. C. Gossard. Spontaneous coherence in a cold exciton gas. *Nature*, 483(7391):584–588, 2012.

[64] M. Baranov. Theoretical progress in many-body physics with ultracold dipolar gases. *Physics Reports*, 464(3):71–111, 2008.

[65] A. Amo, J. Lefrère, S. Pigeon, C. Adrados, C. Ciuti, I. Carusotto, R. Houdré, E. Giacobino, and A. Bramati. Superfluidity of polaritons in semiconductor microcavities. *Nature Physics*, 5(11):805–810, 2009.

[66] A. Amo, D. Sanvitto, F. P. Laussy, D. Ballarini, E. del Valle, M D Martin, A. Lemaître, J. Bloch, D. N. Krizhanovskii, M. S. Skolnick, C. Tejedor, and L. Viña. Collective fluid dynamics of a polariton condensate in a semiconductor microcavity. *Nature*, 457(7227):291–295, 2009.

[67] K. G. Lagoudakis, M. Wouters, M. Richard, A. Baas, I. Carusotto, R. André, Le Si Dang, and B. Deveaud-Plédran. Quantized vortices in an excitonpolariton condensate. *Nature Physics*, 4(9):706–710, 2008.

[68] D. Sanvitto, F. M. Marchetti, M. H. Szymaska, G. Tosi, M. Baudisch, F. P. Laussy, D. N. Krizhanovskii, M. S. Skolnick, L. Marrucci, A. Lemaître, J. Bloch, C. Tejedor, and L. Viña. Persistent currents and quantized vortices in a polariton superfluid. *Nature Physics*, 6(7):527–533, 2010.

[69] S. Utsunomiya, L. Tian, G. Roumpos, C. W. Lai, N. Kumada, T. Fujisawa, M. Kuwata-Gonokami, A. Löffler, S. Höfling, A. Forchel, and Y. Yamamoto. Observation of Bogoliubov excitations in exciton-polariton condensates. *Nature Physics*, 4(9):700–705, 2008.

[70] J. Keeling and N. G. Berloff. Condensed-matter physics: Going with the flow. *Nature*, 457(7227):273–274, 2009.

[71] G. Tosi, G. Christmann, N. G. Berloff, P. Tsotsis, T. Gao, Z. Hatzopoulos, P. G. Savvidis, and J. J. Baumberg. Sculpting oscillators with light within a nonlinear quantum fluid. *Nature Physics*, 8(3):190–194, 2012.

[72] Th. Best, S. Will, U. Schneider, L. Hackermüller, D. van Oosten, I. Bloch, and D.-S. Lühmann. Role of Interactions in Rb87-K40 Bose-Fermi Mixtures in a 3D Optical Lattice. *Physical Review Letters*, 102(3):030408, 2009.

[73] P. G. Lagoudakis, M. D. Martin, J. J. Baumberg, A. Qarry, E. Cohen, and L. N. Pfeiffer. Electron-Polariton Scattering in Semiconductor Microcavities. *Physical Review Letters*, 90(20):206401, 2003.

[74] P. G. Lagoudakis, J. J. Baumberg, M. D. Martin, A. Qarry, E. Cohen, and L. N. Pfeiffer. Electron-polariton scattering, beneficial and detrimental effects. *Physica Status Solidi (C)*, 1(6):1333–1338, 2004.

[75] G. V. Chester. Speculations on Bose-Einstein Condensation and Quantum Crystals. *Physical Review A*, 2(1):256–258, 1970.

[76] E. Kim and M. H. W. Chan. Probable observation of a supersolid helium phase. *Nature*, 427(6971):225–227, 2004.

[77] H. Ouerdane. Analytic model of effective screened Coulomb interactions in a multilayer system. *Journal of Applied Physics*, 110(2):074905, 2011.

[78] H. Haug and S. W. Koch. *Quantum Theory of the Optical and Electronic Properties of Semiconductors*. World Scientific Publishing, Singapore, 3rd

edition, 1994.

[79] Z. Vörös, D. W. Snoke, L. Pfeiffer, and K. West. Direct Measurement of Exciton-Exciton Interaction Energy. *Physical Review Letters*, 103(1):016403, 2009.

[80] M. Wouters and I. Carusotto. Excitations in a Nonequilibrium Bose-Einstein Condensate of Exciton Polaritons. *Physical Review Letters*, 99(14):140402, 2007.

[81] M. Wouters, T. C. H. Liew, and V. Savona. Energy relaxation in one-dimensional polariton condensates. *Physical Review B*, 82(24):245315, 2010.

[82] F. Tassone and Y. Yamamoto. Exciton-exciton scattering dynamics in a semiconductor microcavity and stimulated scattering into polaritons. *Physical Review B*, 59(16):10830–10842, 1999.

[83] A. V. Kavokin, I. A. Shelykh, T. Taylor, and M.M. Glazov. Vertical Cavity Surface Emitting Terahertz Laser. *Physical Review Letters*, 108(19):197401, 2012.

[84] F. Buersgens, R. Kersting, and H.-T. Chen. Terahertz microscopy of charge carriers in semiconductors. *Applied Physics Letters*, 88(11):112115, 2006.

[85] R. M. Woodward, B. E. Cole, V. P. Wallace, R. J. Pye, D. D. Arnone, E. H. Linfield, and M. Pepper. Terahertz pulse imaging in reflection geometry of human skin cancer and skin tissue. *Physics in Medicine and Biology*, 47(21):3853–3863, 2002.

[86] A. G. Davies, A. D. Burnett, W. Fan, E. H. Linfield, and J. E. Cunningham.

Terahertz spectroscopy of explosives and drugs. *Materials Today*, 11(3):18–26, 2008.

[87] D. Dragoman and M. Dragoman. Terahertz fields and applications. *Progress in Quantum Electronics*, 28(1):1–66, 2004.

[88] J. Faist, F. Capasso, D. L. Sivco, C. Sirtori, A. L. Hutchinson, and A. Y. Cho. Quantum cascade laser. *Science*, 264(5158):553–556, 1994.

[89] B. S. Williams. Terahertz quantum-cascade lasers. *Nature Photonics*, 1(9):517–525, 2007.

[90] Y. Todorov, I. Sagnes, I. Abram, and C. Minot. Purcell Enhancement of Spontaneous Emission from Quantum Cascades inside Mirror-Grating Metal Cavities at THz Frequencies. *Physical Review Letters*, 99(22):223603, 2007.

[91] K. V. Kavokin, M. A. Kaliteevski, R. A. Abram, A. V. Kavokin, S. Sharkova, and I. A. Shelykh. Stimulated emission of terahertz radiation by exciton-polariton lasers. *Applied Physics Letters*, 97(20):201111, 2010.

[92] I. G. Savenko, I. A. Shelykh, and M. A. Kaliteevski. Nonlinear Terahertz Emission in Semiconductor Microcavities. *Physical Review Letters*, 107(2):027401, 2011.

[93] E. del Valle and A. V. Kavokin. Terahertz lasing in a polariton system: Quantum theory. *Physical Review B*, 83(19):193303, 2011.

[94] I. Catalano, A. Cingolani, R. Cingolani, M. Lepore, and K. Ploog. Two-photon spectroscopy in GaAs/AlxGa1-xAs multiple quantum wells. *Physical Review B*, 40(2):1312–1315, 1989.

[95] R. Kaindl, D. Hägele, M. Carnahan, and D. Chemla. Transient terahertz spectroscopy of excitons and unbound carriers in quasi-two-dimensional electron-hole gases. *Physical Review B*, 79(4):045320, 2009.

[96] N. Garro, S. P. Kennedy, A. P. Heberle, and R. T. Phillips. Coherent Control of Two-Photon Transitions. *Physica Status Solidi (B)*, 221(1):385–389, 2000.

[97] J. L. Tomaino, A. D. Jameson, Yun-shik Lee, G. Khitrova, H. M. Gibbs, A. C. Klettke, M. Kira, and S. W. Koch. Terahertz excitation of a coherent three-level Λ-type exciton-polariton microcavity mode. *arXiv*, 1112.2185, 2011.

[98] I. G. Savenko, E. B. Magnusson, and I. A. Shelykh. Density-matrix approach for an interacting polariton system. *Physical Review B*, 83(16):165316, 2011.

[99] T. Ostatnický, I. A. Shelykh, and A. V. Kavokin. Theory of polarization-controlled polariton logic gates. *Physical Review B*, 81(12):125319, 2010.

[100] E. L. Ivchenko. *Optical Spectroscopy of Semiconductor Nanostructures*. Alpha Science, Harrow, UK, 2005.

[101] J. G. Bednorz and K. A. Müller. Possible high T_c superconductivity in the Ba-La-Cu-O system. *Zeitschrift für Physik B: Condensed Matter*, 64(2):189–193, 1986.

[102] C. Pfleiderer. Superconducting phases of f -electron compounds. *Reviews of Modern Physics*, 81(4):1551–1624, 2009.

[103] C. C. Tsuei and J. R. Kirtley. Pairing symmetry in cuprate superconductors. *Reviews of Modern Physics*, 72(4):969–1016, 2000.

[104] F. Kagawa, K. Miyagawa, and K. Kanoda. Unconventional critical behaviour in a quasi-two-dimensional organic conductor. *Nature*, 436(7050):534–537, 2005.

[105] M. R. Norman. High-temperature superconductivity in the iron pnictides. *Physics*, 1:21, 2008.

[106] H. K. Onnes. The resistance of pure mercury at helium temperatures. *Commun. Phys. Lab. Univ. Leiden*, 12:120, 1911.

[107] W. Meissner and R. Ochsenfeld. Ein neuer Effekt bei Eintritt der Supraleitfähigkeit. *Die Naturwissenschaften*, 21(44):787–788, 1933.

[108] F. London and H. London. The Electromagnetic Equations of the Supraconductor. *Proceedings of the Royal Society A: Mathematical, Physical and Engineering Sciences*, 149(866):71–88, 1935.

[109] A. B. Pippard. An Experimental and Theoretical Study of the Relation between Magnetic Field and Current in a Superconductor. *Proceedings of the Royal Society A: Mathematical, Physical and Engineering Sciences*, 216(1127):547–568, 1953.

[110] V. L. Ginzburg and L. D. Landau. On the theory of superconductivity. *Soviet Physics JETP*, 20:1064, 1950.

[111] L. P. Gor'kov. Microscopic derivation of the Ginzburg-Landau equations in the theory of superconductivity. *Soviet Physics JETP*, 36:1364, 1959.

[112] E. Maxwell. Isotope Effect in the Superconductivity of Mercury. *Physical Review*, 78(4):477, 1950.

[113] C. Reynolds, B. Serin, W. Wright, and L. Nesbitt. Superconductivity of Isotopes of Mercury. *Physical Review*, 78(4):487, 1950.

[114] H. Fröhlich. Theory of the Superconducting State. I. The Ground State at the Absolute Zero of Temperature. *Physical Review*, 79(5):845–856, 1950.

[115] J. Bardeen, L. Cooper, and J. Schrieffer. Microscopic Theory of Superconductivity. *Physical Review*, 106(1):162–164, 1957.

[116] J. Bardeen, L. N. Cooper, and J. R. Schrieffer. Theory of Superconductivity. *Physical Review*, 108(5):1175–1204, 1957.

[117] W. Corak, B. Goodman, C. Satterthwaite, and A. Wexler. Exponential Temperature Dependence of the Electronic Specific Heat of Superconducting Vanadium. *Physical Review*, 96(5):1442–1444, 1954.

[118] H. Fröhlich. Interaction of Electrons with Lattice Vibrations. *Proceedings of the Royal Society A: Mathematical, Physical and Engineering Sciences*, 215(1122):291–298, 1952.

[119] J. Bardeen and David Pines. Electron-Phonon Interaction in Metals. *Physical Review*, 99(4):1140–1150, 1955.

[120] L. N. Cooper. Bound Electron Pairs in a Degenerate Fermi Gas. *Physical Review*, 104(4):1189–1190, 1956.

[121] L. D. Landau and E. M. Lifshitz. *Quantum Mechanics (Non-Relativistic Theory)*. Pergamon, Oxford, 3rd edition, 1977.

[122] N. N. Bogoliubov. A new method in the theory of superconductivity. *Soviet Physics JETP*, 34:58, 1958.

[123] P. Morel and P. Anderson. Calculation of the Superconducting State Parameters with Retarded Electron-Phonon Interaction. *Physical Review*, 125(4):1263–1271, 1962.

[124] W. Little. Possibility of Synthesizing an Organic Superconductor. *Physical Review*, 134(6A):A1416–A1424, 1964.

[125] V. L. Ginzburg. The Problem of High-Temperature Superconductivity. II. *Soviet Physics Uspekhi*, 13(3):335–352, 1970.

[126] D. Allender, J. Bray, and J. Bardeen. Model for an Exciton Mechanism of Superconductivity. *Physical Review B*, 7(3):1020–1029, 1973.

[127] F. P. Laussy, A. V. Kavokin, and I. A. Shelykh. Exciton-Polariton Mediated Superconductivity. *Physical Review Letters*, 104(10):106402, 2010.

[128] M. J. Bijlsma, B. A. Heringa, and H. T. C. Stoof. Phonon exchange in dilute Fermi-Bose mixtures: Tailoring the Fermi-Fermi interaction. *Physical Review A*, 61(5):053601, 2000.

[129] H. Heiselberg, C. Pethick, H. Smith, and L. Viverit. Influence of Induced Interactions on the Superfluid Transition in Dilute Fermi Gases. *Physical Review Letters*, 85(12):2418–2421, 2000.

[130] M. Kitamura. Non-Linear Integral Equations of the Hammerstein Type. *Progress of Theoretical Physics*, 30(4):435–442, 1963.

[131] A. Vansevenant. The gap equation in superconductivity theory. *Physica D: Nonlinear Phenomena*, 17(3):339–344, 1985.

[132] P. P. Zabreiko and A. I. Povolotskii. On the theory of the Hammerstein equation. *Ukrainian Mathematical Journal*, 22(2):127–138, 1970.

[133] F. P. Laussy, T. Taylor, I. A. Shelykh, and A. V. Kavokin. Superconductivity with excitons and polaritons: review and extension. *Journal of Nanophotonics*, 6(1):064502, 2012.

[134] J. B. Ketterson and S. N. Song. *Superconductivity*. Cambridge University Press, Cambridge, 1999.

[135] X. H. Zheng and D. G. Walmsley. Coulomb repulsion and Tc in BCS theory of superconductivity. *Physical Review B*, 71(13):134512, 2005.

[136] K. H. Bennemann and J. B. Ketterson, editors. *The Physics of Superconductors Vol. I*. Springer, 2003.

[137] G. M. Eliashberg. Interactions between electrons and lattice vibrations in a superconductor. *Soviet Physics JETP*, 11:696, 1960.

[138] M J Holcomb. Finite-temperature real-energy-axis solutions of the isotropic Eliashberg integral equations. *Physical Review B*, 54(9):6648–6660, 1996.

[139] I. A. Shelykh, T. Taylor, and A. V. Kavokin. Rotons in a Hybrid Bose-Fermi System. *Physical Review Letters*, 105(14):140402, 2010.

[140] D. Bohm and D. Pines. A Collective Description of Electron Interactions. I. Magnetic Interactions. *Physical Review*, 82(5):625–634, 1951.

[141] M. Gell-Mann and K. A. Brueckner. Correlation Energy of an Electron Gas at High Density. *Physical Review*, 106(2):364–368, 1957.

[142] P. Nozières and D. Pines. Correlation Energy of a Free Electron Gas. *Physical Review*, 111(2):442–454, 1958.

[143] A. M. Zagoskin. *Quantum Theory of Many-Body Systems*. Springer, New York, 1998.

[144] D. R. Nelson and J. M. Kosterlitz. Universal Jump in the Superfluid Density of Two-Dimensional Superfluids. *Physical Review Letters*, 39(19):1201–1205, 1977.

[145] O. L. Berman, Y. E. Lozovik, D. W. Snoke, and R. D. Coalson. Collective properties of indirect excitons in coupled quantum wells in a random field. *Physical Review B*, 70(23):235310, 2004.

[146] G. Malpuech, D. D. Solnyshkov, H. Ouerdane, M. M. Glazov, and I. A. Shelykh. Bose Glass and Superfluid Phases of Cavity Polaritons. *Physical Review Letters*, 98(20):206402, 2007.

[147] G. Christmann, A. Askitopoulos, G. Deligeorgis, Z. Hatzopoulos, S. I. Tsintzos, P. G. Savvidis, and J. J. Baumberg. Oriented polaritons in strongly-coupled asymmetric double quantum well microcavities. *Applied Physics Letters*, 98(8):081111, 2011.

[148] P. Cristofolini, G. Christmann, S. I. Tsintzos, G. Deligeorgis, G. Konstantinidis, Z. Hatzopoulos, P. G. Savvidis, and J. J. Baumberg. Coupling Quantum Tunneling with Cavity Photons. *Science*, 336:704–707, 2012.

[149] Y. Pomeau and S. Rica. Dynamics of a model of supersolid. *Physical Review Letters*, 72(15):2426–2429, 1994.

[150] M. Matuszewski. Rotonlike Instability and Pattern Formation in Spinor Bose-Einstein Condensates. *Physical Review Letters*, 105(2):020405, 2010.

[151] F. Cinti, P. Jain, M. Boninsegni, A. Micheli, P. Zoller, and G. Pupillo. Supersolid Droplet Crystal in a Dipole-Blockaded Gas. *Physical Review Letters*, 105(13):135301, 2010.

[152] N. Henkel, R. Nath, and T. Pohl. Three-Dimensional Roton Excitations and Supersolid Formation in Rydberg-Excited Bose-Einstein Condensates. *Physical Review Letters*, 104(19):195302, 2010.

[153] M. Matuszewski, T. Taylor, and A. V. Kavokin. Exciton Supersolidity in Hybrid Bose-Fermi Systems. *Physical Review Letters*, 108(6):060401, 2012.

[154] A. F. Andreev and I. M. Lifshitz. Quantum theory of defects in crystals. *Soviet Physics JETP*, 29:1107–1113, 1969.

[155] D. J. Thouless. The flow of a dense superfluid. *Annals of Physics*, 52(3):403–427, 1969.

[156] A. J. Leggett. Can a Solid Be "Superfluid"? *Physical Review Letters*, 25(22):1543–1546, 1970.

[157] E. Kim and M. H. W. Chan. Observation of superflow in solid helium. *Science*, 305(5692):1941–1944, 2004.

[158] K. Baumann, C. Guerlin, F. Brennecke, and T. Esslinger. Dicke quantum phase transition with a superfluid gas in an optical cavity. *Nature*, 464(7293):1301–6, 2010.

[159] R. Mottl, F. Brennecke, K. Baumann, R. Landig, T. Donner, and T. Esslinger. Observation of roton-type mode softening in a quantum gas with cavity-mediated long-range interactions. *arXiv*, 1203.1322, 2012.

[160] E. J. Pratt, B. Hunt, V. Gadagkar, M. Yamashita, M. J. Graf, A. V. Balatsky, and J. C. Davis. Interplay of rotational, relaxational, and shear dynamics in solid He4. *Science*, 332(6031):821–824, 2011.

[161] M. M. Parish, F. M. Marchetti, and P. B. Littlewood. Supersolidity in electron-hole bilayers with a large density imbalance. *Europhysics Letters*, 95(2):27007, 2011.

[162] L. V. Butov, A. A. Shashkin, V. T. Dolgopolov, K. L. Campman, and A. C. Gossard. Magneto-optics of the spatially separated electron and hole layers in GaAs/AlxGa1-xAs coupled quantum wells. *Physical Review B*, 60(12):8753–8758, 1999.

[163] B. Laikhtman and R. Rapaport. Exciton correlations in coupled quantum wells and their luminescence blue shift. *Physical Review B*, 80(19):195513, 2009.

[164] C. Schindler and R. Zimmermann. Analysis of the exciton-exciton interaction in semiconductor quantum wells. *Physical Review B*, 78(4):045313, 2008.

[165] L. Bergé. Wave collapse in physics: principles and applications to light and plasma waves. *Physics Reports*, 303(5-6):259–370, 1998.